

Approximate message-passing decoder and capacity-achieving sparse superposition codes

Jean Barbier[†] and Florent Krzakala^{†,*, \cap}

[†] Laboratoire de Physique Statistique, UMR 8550 CNRS & UPMC,
Ecole Normale Supérieure, 24 rue Lhomond, 75005 Paris, France.

* Université Pierre et Marie Curie, Sorbonne Universités.

\cap Laboratoire de physico-chimie théorique, UMR 7083 *Gulliver* ESPCI & CNRS,
ESPCI ParisTech, 10 rue Vauquelin, 75005 Paris, France.

Email: jean.barbier@ens.fr, florent.krzakala@ens.fr

Abstract

We study the approximate message-passing decoder for sparse superposition coding on the additive white Gaussian noise channel and extend our preliminary work [1]. While this coding scheme asymptotically reach the Shannon capacity, we show that our iterative decoder is limited by a phase transition similar to what happen in LDPC codes. We present and study two solutions to this problem, that both allow to reach the Shannon capacity: i) a non constant power allocation and ii) the use of spatially coupled codes. We also present extensive simulations that suggest that spatial coupling is more robust and allows for better reconstruction at finite code lengths. Finally, we show empirically that the use of a fast Hadamard-based operator allows for an efficient reconstruction, both in terms of computational time and memory, and the ability to deal with large signals.

Index Terms

sparse superposition codes, error-correcting codes, approximate message-passing, spatial coupling, power allocation, compressed sensing, capacity achieving, state evolution, replica analysis, fast Hadamard operator.

CONTENTS

I	Introduction	2
I-A	Related works	2
I-B	Main contributions of the present study	2
I-C	Outline	3
II	Sparse superposition codes	3
III	The approximate message-passing algorithm	5
III-A	Derivation from belief propagation	6
III-B	The fast Hadamard-based sensing operator	9
III-C	Further simplifications for random matrices with zero mean	11
IV	State evolution analysis for random i.i.d dense operators with constant power allocation	12
V	State evolution analysis for spatially coupled i.i.d operators or power allocation	16
V-A	Derivation of the state evolution in the spatially coupled operator case	16
V-B	State evolution with power allocation	19
VI	Replica analysis	20
VI-A	Replica analysis with uniform power allocation	20
VI-B	The link between replica and state evolution analysis	23
VI-C	Large section limit of the superposition codes	24
VI-D	Results from the replica analysis	25
VII	Optimality of AMP reconstruction with a proper power allocation	26
VIII	Numerical experiments for finite size signals	29
IX	Conclusion and future works	31
	References	32

I. INTRODUCTION

The error correction scheme called sparse superposition codes has originally been introduced and studied in [2–4] by Barron and Joseph who proved the scheme to be capacity achieving over the Additive White Gaussian Noise (AWGN) channel under Maximum A Posteriori (MAP) decoding. In [2–4], an iterative decoder called *adaptive successive decoder* was presented, which was later improved in [5, 6] by soft thresholding methods. The idea is to decode a sparse vector with a special block structure over the AWGN channel, represented in Fig. 1. With these decoders, the scheme was proved to be capacity achieving, together with the use of power allocation. However, finite blocklength performances were far from ideal. In fact, it seemed that the asymptotic results could be reproduced at any reasonable finite lengths.

We have proposed the Approximate Message-Passing (AMP) decoder associated with sparse superposition codes in [1]. This decoder was shown to have much better performances; in fact they allowed better decoding performances for finite length even without power allocation. The goal of the present contribution is to complete and extend the short presentation in [1]. In particular, we present two modifications of sparse superposition codes that allow AMP to be asymptotically capacity achieving as well, while retaining good finite block length properties. The first one is the addition of power allocation to sparse superposition codes, and the second one the use of spatial coupling, which we find even more promising.

We also present extensive numerical simulations, and a study of a practical scheme with Hadamard operators. The overall scheme allows to practically reach near-to-capacity rates.

A. Related works

The phenomenology of these codes with AMP decoding, in particular the sharp phase transitions different between MAP and AMP, has many similarities with what appears in Low Density Parity Check codes (LDPC) [7].

It is actually in the context of LDPC codes that spatial coupling has been introduced [8, 9] to actually deal with this phase transition phenomenon that blocks the convergence of message-passing based decoders. These similarities are not a priori trivial because LDPC are codes over finite fields, the sparse superposition codes scheme works in the continuous framework and LDPC are decoded by loopy Belief-Propagation (BP) whereas sparse superposition codes are decoded by AMP which is a Gaussian approximation of loopy BP. However, they arise due to a deep connection to compressed sensing, where these phenomena (phase transition, spatial coupling, ...) have been studied as well [10–13] and we shall make use of this connection extensively.

The AMP algorithm, which stands at the roots of our approach, is a simple relaxation of loopy BP. While the principle behind AMP has been used for a long time, the present form has been originally derived for compressed sensing [14, 15] and is naturally applied to sparse superposition codes as this scheme can be interpreted as a compressed sensing problem with structured sparsity. The state evolution technique [16] is unfortunately not rigorous for the present AMP approach because of the structured sparsity of the signal, but in spite of that, we conjecture that it is exact.

Note that reconstruction of structured signals is a new trend in compressed sensing theory that aims at going beyond simple sparsity by introducing more complex structures in the vector that is to be reconstructed. Other examples include group sparsity or tree structure in the wavelet coefficients in image reconstruction [17]. Finally, we report that upon completion of this manuscript, we became aware of the very recent work of Rush, Greig and Venkataramanan [18] who also studied AMP decoding in superposition codes using power allocation. Using the same technics as in [16], they prove rigorously that AMP was capacity-achieving if a proper power allocation is used. This strengthens the claims that AMP is the tool of choice in the present problem. We will see, however, that spatial coupling leads to even better results at finite size.

B. Main contributions of the present study

The main original results of the present study are listed below. In particular, we shall also extend and give a detailed presentation of the previous short publications by the authors [1, 19].

- A detailed derivation of the AMP decoder for sparse superposition codes for a generic power allocation, which was first presented in [1]. The derivation is self-contained and starts all the way from the canonical loopy BP equations.
- An analysis of the performance of the AMP decoder from the state evolution recursions, again presented without derivation in [1]. Here this is done in full generality with and without power allocation, and with and without spatial coupling. Note that, while we do not attempt to be mathematically rigorous in this contribution, the state evolution approach has been shown to be rigorously exact for many similar estimation problems [16, 20]. The present approach does not verify the hypothesis required for the proofs to be valid because of the structured sparsity of the signal, but nevertheless we conjecture that the analysis remains exact. It is shown in particular that AMP, for simple sparse superposition codes, suffers from a phenomenon similar to those of BP with LDPC codes: there is a sharp transition —different from the optimum one of the code itself— beyond which its performance suddenly decays.
- An analysis of the optimum performance of sparse superposition codes using the non-rigorous replica method, a powerful heuristic tool from statistical physics [21, 22]. This leads in particular to a single-letter formulation of the Minimal Mean Square Error (MMSE) which we conjecture to be exact. The connection and consistency with the results coming from the state evolution approach is also underlined. Again, this was only partially presented in [1].

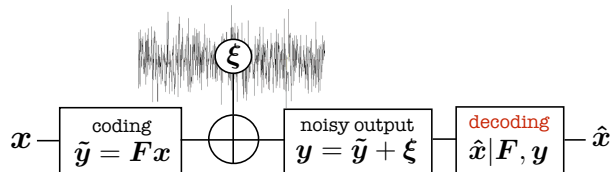


Fig. 1. Sending information through the AWGN channel with superposition codes: the message \mathbf{x} , created such that it has only a single non zero element in each of its L sections, is first coded by a linear transform, $\tilde{\mathbf{y}} = \mathbf{F}\mathbf{x}$. It is then sent through the AWGN channel that adds an i.i.d Gaussian noise ξ with zero mean and a given variance Δ to each components. The receptor gets the corrupted message \mathbf{y} and must estimate $\hat{\mathbf{x}}$ as close as possible from \mathbf{x} from the knowledge of \mathbf{F} and \mathbf{y} . Perfect decoding happens if $\hat{\mathbf{x}} = \mathbf{x}$.

- We present an analysis of the large section limit (partial results were only stated in [1]) for the behavior of AMP, and compute its limit rate, the so called BP threshold $R_{BP} < C$ where C is the Shannon capacity of the channel. As a by-product, we reconfirm, using the replica method, that these codes are Shannon capacity achieving.
- We also show that, with a proper power allocation, the BP threshold that was blocking the AMP decoder disappears so that AMP becomes asymptotically capacity achieving over the AWGN in a proper asymptotic limit.
- Building on the connection with compressed sensing in [11–13] we also show that the use of spatial coupling [8] for sparse superposition codes is an alternative way to obtain capacity achieving performances with AMP.
- We also present an extensive numerical study at finite blocklength, showing that despite improvements of the scheme thanks to power allocation, a properly designed spatially coupled coding matrix seems to allow better performances and robustness to noise for decoding over finite size signals.
- We also discuss a more practical scheme where the random operators of the sparse superposition codes are replaced by fast operators based on an Hadamard construction. We show that this allows a close to linear time algorithm able to deal with very large signals, yet performing very well at large rate for finite signals. These results were only hinted at in [19]. We study the efficiency of these operators combined with sparse superposition codes with or without spatial coupling.

Finally, we note that our work differs from the mainstream of existing literature. While a large part of the existing coding theory literature provides theorems, part of our work—that using the replica method—is based on statistical physics methods that are conjectured to give exact results. While many results obtained with these methods on a variety of problems have indeed been proven later on, a general proof that these methods are rigorous is not yet known. Note, however, that the state evolution technique (also called cavity method in statistical physics) has been turned into a rigorous tool under controls in many similar cases [16, 20], though not yet in the vectorial case discussed in the present contribution. We thus expect that both the replica analysis and the state evolution results are exact and believe it is only a matter of time before they are fully proven.

C. Outline

The present paper is constructed as follows. We start by introducing the setting of sparse superposition codes in Sec. II. The third section is dedicated to a step-by-step derivation of the AMP decoder for sparse superposition codes and the fast Hadamard spatially coupled operator construction. Sec. IV gives the derivation of the state evolution recursions for AMP in the simpler setting of constant power allocation case without spatial coupling and starting from the AMP algorithm. The Sec. V are the results of the state evolution analysis in the spatially coupled case, actually equivalent to the non constant power allocation case in terms of the state evolution derivation. Some numerical experiments are performed to confirm the approximate validity of the state evolution analysis for predicting the behavior of the decoder with Hadamard based operators. Sec. VI give the full derivation of the replica analysis and main results extracted from it, basically a potential function that contains the information on the optimality of the scheme and the transitions blocking the convergence if present. In Sec. VII, starting from this previous replica analysis, we show how to choose the power allocation such that superposition codes are capacity achieving with no need of spatial coupling. Finally, Sec. VIII summarizes the results of our numerical studies of the scheme, such as the efficiency of spatial coupling with Hadamard based operators, and the comparisons between power allocation and spatial coupling strategies. Finally the last section concludes and gives some interesting open questions from our point of view, followed by the acknowledgments and related references.

In what follows, all the vectors will be denoted with bold symbols, the matrices with capital bold symbols. Any sum or product index starts from 1 if not specified. The notation $x \sim P(\theta)$ means that x is a random variable with distribution $P(\theta)$ that can depend on some hyperparameters θ .

II. SPARSE SUPERPOSITION CODES

Suppose you want to send a generic message $\tilde{\mathbf{x}}$ made of L symbols, each symbol belonging to an alphabet composed of B letters through an AWGN channel: $\tilde{\mathbf{x}} := \{\tilde{x}_l : \tilde{x}_l \in \{1, \dots, B\} \forall l \in \{1, \dots, L\}\}$. Starting from a standard binary representation of $\tilde{\mathbf{x}}$, it is of course trivial to encode it in this form.

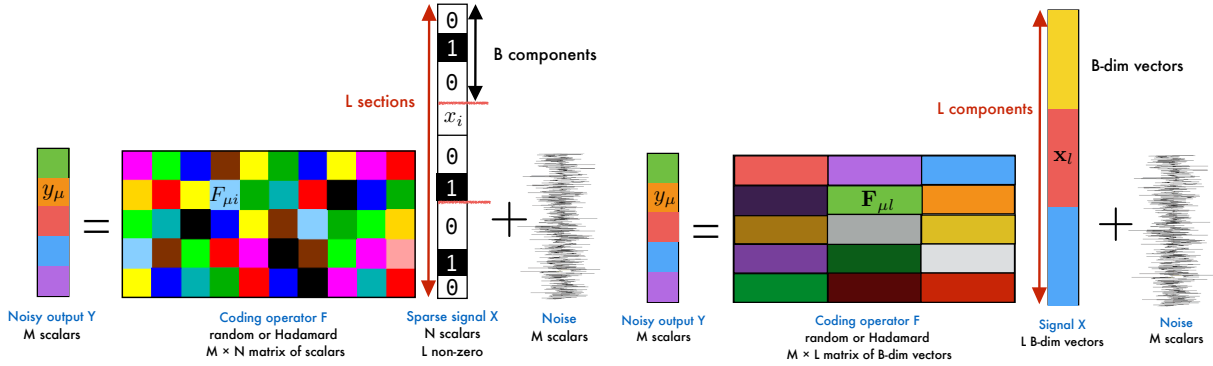


Fig. 2. **Left** : Representation of the estimation problem associated to the decoding of the sparse signal over the AWGN channel. All variables in the same section $\{x_i : i \in \mathbf{I}\}$ are strongly correlated due to the hard constraint that only one of them can be positive (or 1 in this example). The matrix elements are scalars just as the signal components. **Right** : Reinterpreting the same problem in terms of B -d variables. Now, the matrix elements of the previous figure are grouped to form B -d vectors that are applied (using the usual scalar product for vectors) on the associated B -d vectors representing the new components of the signal. In this new setting, all signal vectorial elements are uncorrelated.

An alternative and highly *sparse* representation is given by the sparse superposition codes scheme: the representation \mathbf{x} of this message $\tilde{\mathbf{x}}$ is made of L sections of size B , where only a *unique* value is $\neq 0$ in each section (that we will consider positive as it can be interpreted as an input energy in the channel) at the location corresponding to the original symbol: If the i^{th} component of the original message $\tilde{\mathbf{x}}$ is the k^{th} symbol of the alphabet, the i^{th} section of \mathbf{x} contains only zeros, except at the position k , where there is a positive value (the value depends on the power allocation).

As an example, in the simplest setting where the *power allocation* is $c_l = 1 \forall l \in \{1, \dots, L\}$ (where c_l is the positive constant appearing in the l^{th} section), if $\tilde{\mathbf{x}} = [a, c, b]$, where the alphabet has only three symbols $\{a, b, c\}$, then $\mathbf{x} = [[100], [001], [010]]$. The l^{th} section of \mathbf{x} will be denoted $\mathbf{x}_l := \{x_i : i \in \mathbf{I}\}$ where \mathbf{I} is the set of indices corresponding to the components of \mathbf{x} in the l^{th} section.

In sparse superposition codes, \mathbf{x} is then encoded through a linear transform by application of an operator \mathbf{F} of dimension $M \times N$ to obtain a codeword $\tilde{\mathbf{y}}$ of dimension M : $\tilde{\mathbf{y}} = \mathbf{F}\mathbf{x}$, which is then sent through the Gaussian noisy channel. This is summarized in Fig. 1.

The dimension of the operator is linked to the dimension B of a section and the coding rate in bits per-channel use R , from which we deduce the rate as a function of the operator size. Defining $K := \log_2(B^L)$ as the number of informative bits in the signal \mathbf{x} made of L sections of size B :

$$R := K/M = L \log_2(B)/(\alpha N) = \log_2(B)/(B\alpha) \quad (1)$$

$$\Leftrightarrow \alpha := M/N = \log_2(B)/(RB) \quad (2)$$

In what follows we will concentrate on independent and identically distributed (i.i.d) Gaussian \mathbf{F} elements with 0 mean and variance Δ , in order to be able to obtain analytical results. We fix the total power sent through the channel $P := \|\tilde{\mathbf{y}}\|_2^2 = 1/M \sum_{\mu} \tilde{y}_{\mu}^2$ to $P = 1$ by a proper rescaling of the variance of the elements of \mathbf{F} . The only relevant parameter is thus the signal-to-noise ratio:

$$\text{snr} := P/\sigma^2 = 1/\sigma^2 \quad (3)$$

where σ^2 is the variance of the Gaussian noise in the AGWN. According to the celebrated Shannon formula [23], the capacity of the power constrained AWGN channel is

$$C = \frac{1}{2} \log_2(1 + \text{snr}). \quad (4)$$

The codeword $\tilde{\mathbf{y}}$ is sent through the Gaussian noisy channel which outputs a corrupted version \mathbf{y} to the receiver. So the overall channel model is given by (see Fig. 1):

$$\mathbf{y} = \tilde{\mathbf{y}} + \boldsymbol{\xi} = \mathbf{F}\mathbf{x} + \boldsymbol{\xi}, \quad \xi_{\mu} \sim \mathcal{N}_{0, \sigma^2} \quad \forall \mu \in \{1, \dots, M\}, \quad (5)$$

where $\mathcal{N}_{u, \sigma^2}$ is a Gaussian distribution of mean u and variance σ^2 .

Let us turn now our attention to the decoding task, which we discuss in Fig. 2. It is essentially a sparse linear estimation problem where we know \mathbf{y} and need to estimate a sparse solution of $\mathbf{y} = \mathbf{F}\mathbf{x} + \boldsymbol{\xi}$. However the problem is different from the canonical compressed sensing problem [24] in that the elements of \mathbf{x} are correlated by the constraint that only a single element in each section is non-zero. We thus prefer to think of the problem as a multidimensional one, as discussed in [1]. Each section $l \in \{1, 2, \dots, L\}$ of B variables in $\tilde{\mathbf{x}}$ is interpreted as a *single* B -dimensional (B -d) variable for which we have a strong prior information: it is zero in all dimensions *but* one where there is a fixed positive value. Given its length, we thus know the vector must point in only one of the directions of the hypercube of dimension B . With this new setting, instead of

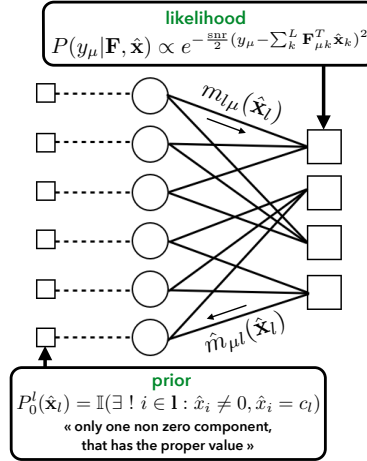


Fig. 3. Factor graph representation associated to sparse superposition codes. It is a bipartite graph where the variables estimates $\{\hat{\mathbf{x}}_l : l \in \{1, \dots, L\}\}$ are represented by circles, the constraints (or factors) by squares. The variables are constrained by the M factors on the right side which represent the linear coding constraints (called the likelihood factors) that enforce the system $\mathbf{y} = \mathbf{F}\hat{\mathbf{x}}$ to be fulfilled up to Gaussian fluctuations due to the Gaussian noise. The prior constraints on the left side enforce each section to have only one non-zero value (that must be the value fixed by the power allocation) in each section. In the non spatially coupled operator case, the variables are connected to all the likelihood factors and vice versa. In the spatially coupled case, only to a finite fraction that depends on the coupling window w , see Fig. 5. The factor-to-node $\hat{m}_{\mu l}(\hat{\mathbf{x}}_l)$ and node-to-factor $m_{l\mu}(\hat{\mathbf{x}}_l)$ cavity messages are represented. The two messages should sit on the same edge as they depend on the same variable and factor but we put them on distinct edges for readability purpose.

dealing with a N -d vector $\tilde{\mathbf{x}}$ with elements x_i , we deal with a L -d vector \mathbf{x} whose elements \mathbf{x}_l are B -d vectors. We define $\mathbf{F}_{\mu l} := \{F_{\mu i} : i \in \mathbf{I}\}$ as the vector of elements of the matrix \mathbf{F} that act on \mathbf{x}_l (see Fig. 2).

In this setting, the decoding problem becomes exactly of the kind considered in the Bayesian approach to compressed sensing, see e.g. [11, 12, 15, 25, 26] and we can thus directly apply these techniques to the present problem. Other analogies between compressed sensing and error correction over the AWGN exist in the literature such as [27]. For the rest of the paper, we consider that the true snr is accessible to the channel user, and thus can be used in the algorithm.

We will be interested in two error estimators, namely the biased mean-squared error (MSE) \tilde{E} and the section error rate SER. They are defined respectively as the MSE of the 1-d variables (the term biased comes from the fact that in application we are interested in the error related to the sections) and the fraction of wrongly reconstructed sections:

$$\tilde{E} = 1/N \sum_i^N (x_i - \hat{x}_i)^2 \quad (6)$$

$$\text{SER} = 1/L \sum_l^L \mathbb{I}(\mathbf{x}_l \neq \hat{\mathbf{x}}_l) \quad (7)$$

where $\mathbb{I}(A)$ is the indicator function of the event A which is one if A happens to be true, zero else and $\hat{\mathbf{x}} := [\hat{\mathbf{x}}_1, \dots, \hat{\mathbf{x}}_L] = [\hat{x}_1, \dots, \hat{x}_N]$ is the estimate of the signal by the decoder.

III. THE APPROXIMATE MESSAGE-PASSING ALGORITHM

As the message \mathbf{x} is binary, one could think about BP as a good decoder. Let's write the canonical BP equations, associated to the factor graph Fig. 3, for the B -d variables to understand why it is not appropriate in the present context:

$$\hat{m}_{\mu l}(\hat{\mathbf{x}}_l) = \frac{1}{\hat{z}_{\mu l}} \sum_{\{\hat{\mathbf{x}}_k\}_{k \neq l}}^{2^{B(L-1)}} e^{-\frac{\text{snr}}{2} (\sum_{k \neq l}^{L-1} \mathbf{F}_{\mu k}^T \hat{\mathbf{x}}_k + \mathbf{F}_{\mu l}^T \hat{\mathbf{x}}_l - y_\mu)^2} \prod_{k \neq l}^{L-1} m_{k\mu}(\hat{\mathbf{x}}_k) \quad (8)$$

$$m_{l\mu}(\hat{\mathbf{x}}_l) = \frac{1}{z_{l\mu}} P_0^l(\hat{\mathbf{x}}_l) \prod_{\nu \neq \mu}^{M-1} \hat{m}_{\nu l}(\hat{\mathbf{x}}_l) \quad (9)$$

where the Greek letters are associated to the factors that correspond to the constraint that $\hat{\mathbf{x}}$ must verify the system (5) up to Gaussian fluctuations (due to the AWGN), the roman ones to the variables nodes.

The basic objects in this approach are the so-called cavity messages $\{\hat{m}_{\mu l}(\hat{\mathbf{x}}_l), m_{l\mu}(\hat{\mathbf{x}}_l)\}$ (the set of factor-to-node and node-to-factor messages respectively) which are probability distributions from $\mathbb{R}^B \rightarrow [0, 1]$ in modified graphical models: $\hat{m}_{\mu l}(\hat{\mathbf{x}}_l)$ is the distribution of the estimator $\hat{\mathbf{x}}_l$ in a graphical model where the variable node associated to $\hat{\mathbf{x}}_l$ is only connected to the μ^{th} factor node, $m_{l\mu}(\hat{\mathbf{x}}_l)$ is its probability in a graph where $\hat{\mathbf{x}}_l$ is connected to all the factor nodes except the μ^{th} one. The distributions can be computed iteratively in an exact way on a tree, or approximately on a generic graph (in this case, the

<pre> 1: $t \leftarrow 0$ 2: $\delta \leftarrow \epsilon + 1$ 3: while $t < t_{Max}$ and $\delta > \epsilon$ do 4: $\Theta_\mu^{t+1} \leftarrow \sum_c^{L_c} \tilde{O}_\mu(\mathbf{v}_c^t)$ 5: $w_\mu^{t+1} \leftarrow \sum_c^{L_c} O_\mu(\mathbf{a}_c^t) - \Theta_\mu^{t+1} \frac{y_\mu - w_\mu^t}{1/\text{snr} + \Theta_\mu^t}$ 6: $\Sigma_i^{t+1} \leftarrow \left[\sum_r^{L_r} \tilde{O}_i \left([1/\text{snr} + \Theta_r^{t+1}]^{-1} \right) \right]^{-1/2}$ 7: $R_i^{t+1} \leftarrow a_i^t + (\Sigma_i^{t+1})^2 \sum_r^{L_r} O_i \left(\frac{y_r - w_r^{t+1}}{1/\text{snr} + \Theta_r^{t+1}} \right)$ 8: $v_i^{t+1} \leftarrow f_{c_i} \left((\Sigma_{l_i}^{t+1})^2, \mathbf{R}_{l_i}^{t+1} \right)$ 9: $a_i^{t+1} \leftarrow f_{a_i} \left((\Sigma_{l_i}^{t+1})^2, \mathbf{R}_{l_i}^{t+1} \right)$ 10: $t \leftarrow t + 1$ 11: $\delta \leftarrow 1/N \sum_i^N (a_i^t - a_i^{t-1})^2$ 12: end while 13: return $\{a_i\}$ </pre>	<pre> 1: $t \leftarrow 0$ 2: $\delta \leftarrow \epsilon + 1$ 3: while $t < t_{Max}$ and $\delta > \epsilon$ do 4: $\Theta_\mu^{t+1} \leftarrow \sum_i^N F_{\mu i}^2 v_i^t$ 5: $w_\mu^{t+1} \leftarrow \sum_i^N F_{\mu i} a_i^t - \Theta_\mu^{t+1} \frac{y_\mu - w_\mu^t}{1/\text{snr} + \Theta_\mu^t}$ 6: $\Sigma_i^{t+1} \leftarrow \left[\sum_\mu^M \frac{F_{\mu i}^2}{1/\text{snr} + \Theta_\mu^{t+1}} \right]^{-1/2}$ 7: $R_i^{t+1} \leftarrow a_i^t + (\Sigma_i^{t+1})^2 \sum_\mu^M F_{\mu i} \frac{y_\mu - w_\mu^{t+1}}{1/\text{snr} + \Theta_\mu^{t+1}}$ 8: $v_i^{t+1} \leftarrow f_{c_i} \left((\Sigma_{l_i}^{t+1})^2, \mathbf{R}_{l_i}^{t+1} \right)$ 9: $a_i^{t+1} \leftarrow f_{a_i} \left((\Sigma_{l_i}^{t+1})^2, \mathbf{R}_{l_i}^{t+1} \right)$ 10: $t \leftarrow t + 1$ 11: $\delta \leftarrow 1/N \sum_i^N (a_i^t - a_i^{t-1})^2$ 12: end while 13: return $\{a_i\}$ </pre>
--	---

Fig. 4. The AMP decoder for sparse superposition codes written in two different equivalent forms. The first form underlines how AMP is operating when spatially coupled operators are used instead of matrices and takes advantage from this structure. The second form is more easy to read and explicit the operations done by the operators in the first form. This form can be less efficient than the first if many blocks are only zeros as in the spatially coupled matrices due to their sparsity. l_i is the index of the section to which the i^{th} 1-d variable belongs to. ϵ is the accuracy for convergence and t_{Max} the maximum number of iterations. A suitable initialization for the quantities is ($a_i^{t=0} = 0$, $v_i^{t=0} = \rho\sigma^2$, $w_\mu^{t=0} = y_\mu$). Once the algorithm has converged, i.e. the quantities do not change anymore from iteration to iteration, the estimate of the i^{th} signal component is a_i^t .

procedure is called loopy BP instead of BP because of the loops present in a generic graph, which is therefore not a tree). The terminology of cavity messages, referring to the procedure of digging cavities by erasing nodes or factors in the original factor graph to define new marginal probability distributions, comes from the physics vocabulary. This is because the BP algorithm can be understood as the cavity method of statistical physics of disordered systems (an asymptotic statistical analysis, referred to as the state evolution analysis in the present context) applied to single instance problems.

The problem with loopy BP for sparse superposition codes is now clear, the sum that has to be performed is over an exponential number of terms, which comes from the fact that the underlying factor graph is densely connected. In addition there are $2MN$ messages to deal with, which is way too many. It would become quickly intractable for even small signals. BP is efficient only when the factor graph defining the inference problem to be solved has a low average connectivity like in LDPC codes.

The AMP is here to face this problem and go beyond BP for dense graphs. It is a message-passing algorithm originally derived in its modern form for compressed sensing [11, 12, 16, 28] where one writes the BP equations on a fully connected factor graph with linear constraints ((8), (9) for sparse superposition codes) and then expands them up to the second order in the interaction terms, as we will derive it. It can also be seen as a special case of the non-parametric BP algorithm [29] in the case where one takes only one Gaussian per message in the parametrization.

In this approximation, the variables that are here discrete $\in \{0, 1\}$ are estimated by continuous variables. Their associated marginals are thus densities over \mathbb{R} . It is difficult to store these distributions if not properly parametrized. AMP being a second order Gaussian approximation of the original equations, these densities are Gaussian distributions naturally parametrized by only two vectors per message: its mean and variance vectors (the vectors of mean and variances of the components of the section). In the present derivation, the AMP algorithm is parametrized by mean and variance estimates of different quantities: \mathbf{w}^t is an estimation of the codeword \mathbf{y} (Θ^t its vector of associated variances), \mathbf{R}^t is the estimation of the message before the prior knowledge has been taken into account by applying the denoisers $\{f_{a_i}, f_{c_i}\}$, which is thus the average with respect to the likelihood, $(\Sigma^t)^2$ the associated variances. Finally \mathbf{a}^t is the estimation of \mathbf{x} with all the information available at time t (the average with respect to the posterior), \mathbf{v}^t its posterior variance that should go to zero in the successful decoding case.

A. Derivation from belief propagation

The following generic derivation is very close to that of [12] albeit in the present case it is done in a framework where the variables for which we know the prior are B -d instead of the 1-d ones (for which we want to derive closed equations). It starts from the usual loopy BP equations in the continuous framework:

$$\hat{m}_{\mu l}(\hat{\mathbf{x}}_l) = \frac{1}{\hat{z}_{\mu l}} \int \left[\prod_{k \neq l}^{L-1} d\hat{\mathbf{x}}_k m_{k\mu}(\hat{\mathbf{x}}_k) \right] e^{-\frac{\text{snr}}{2} (\sum_{k \neq l}^{L-1} \mathbf{F}_{\mu k}^T \hat{\mathbf{x}}_k + \mathbf{F}_{\mu l}^T \hat{\mathbf{x}}_l - y_\mu)^2} \quad (10)$$

$$m_{l\mu}(\hat{\mathbf{x}}_l) = \frac{1}{z_{l\mu}} P_0^l(\hat{\mathbf{x}}_l) \prod_{\gamma \neq \mu}^{M-1} \hat{m}_{\gamma l}(\hat{\mathbf{x}}_l) \quad (11)$$

where $d\hat{\mathbf{x}}_k := \prod_{i \in \mathbf{k}} dx_i$. These intractable equations must be simplified. We remind that we fix the power to be 1 by the following scaling: $F_{\mu i} \in O(1/\sqrt{L}) \xrightarrow{L \rightarrow \infty} 0$. This allows to expand the previous equations. We need to apply the Hubbard-Stratanovitch transform to $w := \sum_{k \neq l}^{L-1} \mathbf{F}_{\mu k}^T \hat{\mathbf{x}}_k$ to simplify (10):

$$e^{-\frac{w^2}{2}} = \sqrt{\frac{\text{snr}}{2\pi}} \int d\lambda e^{-\frac{\lambda^2 \text{snr}}{2} + i \text{snr} \lambda w} \quad (12)$$

$$\rightarrow \hat{m}_{\mu l}(\hat{\mathbf{x}}_l) = \frac{\sqrt{\text{snr}}}{\sqrt{2\pi} \hat{z}_{\mu l}} e^{-\frac{\text{snr}}{2} (\mathbf{F}_{\mu l}^T \hat{\mathbf{x}}_l - y_\mu)^2} \int d\lambda e^{-\frac{\lambda^2 \text{snr}}{2}} \prod_{k \neq l}^{L-1} \left[\int d\hat{\mathbf{x}}_k m_{k\mu}(\hat{\mathbf{x}}_k) e^{\text{snr} \mathbf{F}_{\mu k}^T \hat{\mathbf{x}}_k (y_\mu - \mathbf{F}_{\mu l}^T \hat{\mathbf{x}}_l + i\lambda)} \right] \quad (13)$$

To define the approximate messages Gaussian parametrization, we need the following vectorial objects:

$$\mathbf{a}_\square := \int \hat{\mathbf{x}} m_\square(\hat{\mathbf{x}}) d\hat{\mathbf{x}}, \quad \mathbf{v}_\square := \int \hat{\mathbf{x}}^2 m_\square(\hat{\mathbf{x}}) d\hat{\mathbf{x}} - \mathbf{a}_\square^2 \quad (14)$$

where the square \bullet^2 is an elementwise operation as the inverse operation \bullet^{-1} used later on. Expanding (13), keeping only the terms up to $O(1/L)$ and approximating the result by an exponential, we get:

$$\hat{m}_{\mu l}(\hat{\mathbf{x}}_l) = \frac{\sqrt{\text{snr}}}{\sqrt{2\pi} \hat{z}_{\mu l}} e^{-\frac{\text{snr}}{2} (\mathbf{F}_{\mu l}^T \hat{\mathbf{x}}_l - y_\mu)^2} \int d\lambda e^{-\frac{\text{snr} \lambda^2}{2}} \prod_{k \neq l}^{L-1} \left[e^{\mathbf{a}_{k\mu}^T \mathbf{F}_{\mu k} \text{snr} (y_\mu - \mathbf{F}_{\mu l}^T \hat{\mathbf{x}}_l + i\lambda) + \frac{\mathbf{v}_{k\mu}^T \mathbf{F}_{\mu k}^2 \text{snr}^2}{2} (y_\mu - \mathbf{F}_{\mu l}^T \hat{\mathbf{x}}_l + i\lambda)^2} \right] \quad (15)$$

The Gaussian integral over λ can now be performed, and putting all the $\hat{\mathbf{x}}_l$ independent terms in the normalization constant $\hat{z}_{\mu l}$ we obtain:

$$\hat{m}_{\mu l}(\hat{\mathbf{x}}_l) = \frac{1}{\hat{z}_{\mu l}} e^{-\frac{1}{2} \mathbf{A}_{\mu l}^T \hat{\mathbf{x}}_l^2 + \mathbf{B}_{\mu l}^T \hat{\mathbf{x}}_l}, \quad \hat{z}_{\mu l} = \prod_{i \in \mathbf{l}} \sqrt{\frac{2\pi}{A_{\mu i}}} e^{\frac{B_{\mu i}^2}{2A_{\mu i}}} \quad (16)$$

$$\mathbf{A}_{\mu l} := \frac{\mathbf{F}_{\mu l}^2}{1/\text{snr} + \sum_{k \neq l}^{L-1} \mathbf{v}_{k\mu}^T \mathbf{F}_{\mu k}^2}, \quad \mathbf{B}_{\mu l} := \frac{\mathbf{F}_{\mu l} (y_\mu - \sum_{k \neq l}^{L-1} \mathbf{F}_{\mu k}^T \mathbf{a}_{k\mu})}{1/\text{snr} + \sum_{k \neq l}^{L-1} \mathbf{v}_{k\mu}^T \mathbf{F}_{\mu k}^2} \quad (17)$$

We deduce the other message expression:

$$m_{l\mu}(\hat{\mathbf{x}}_l) = \frac{1}{z_{l\mu}} P_0^l(\hat{\mathbf{x}}_l) e^{-\frac{1}{2} (\hat{\mathbf{x}}_l^T \sum_{\gamma \neq \mu}^{M-1} \mathbf{A}_{\gamma l} + \hat{\mathbf{x}}_l^T \sum_{\gamma \neq \mu}^{M-1} \mathbf{B}_{\gamma l})}, \quad z_{l\mu} = \int d\hat{\mathbf{x}}_l P_0^l(\hat{\mathbf{x}}_l) e^{-\frac{1}{2} (\hat{\mathbf{x}}_l^T \sum_{\gamma \neq \mu}^{M-1} \mathbf{A}_{\gamma l} + \hat{\mathbf{x}}_l^T \sum_{\gamma \neq \mu}^{M-1} \mathbf{B}_{\gamma l})} \quad (18)$$

where sums of the form $\sum_\gamma^B \Gamma_{\gamma i} := \left\{ \sum_\gamma^B \Gamma_{\gamma i} : i \in \mathbf{l} \right\}$ are vectors of size B . We now have projected the set of cavity messages onto Gaussian distributions, fully parametrized by their first and second moments.

We define l_i (\mathbf{l}_i) as the B -d variable index (respectively the set of indices) to which the i^{th} 1-d variable belongs to. We can now define a probability measure over a B -d variable: $m_B((\Sigma_l)^2, \mathbf{R}_l, \hat{\mathbf{x}})$ and the corresponding 1-d variables: $\{m_1((\Sigma_{l_i})^2, \mathbf{R}_{l_i}, \hat{x}_i) : i \in \mathbf{l}\}$ are the marginals of the 1-d variables in the associated section. We also define the associated vector of averages \mathbf{f}_{a_i} and variances \mathbf{f}_{c_i} over these marginals:

$$m_B((\Sigma_l)^2, \mathbf{R}_l, \hat{\mathbf{x}}) := \frac{1}{z((\Sigma_l)^2, \mathbf{R}_l)} P_0^l(\hat{\mathbf{x}}) e^{-([\hat{\mathbf{x}}_l - \mathbf{R}_l]^2)^T (2\Sigma_l^2)^{-1}} \quad (19)$$

$$m_1((\Sigma_{l_i})^2, \mathbf{R}_{l_i}, \hat{x}_i) := \int \prod_{j \in \mathbf{l}_i: j \neq i}^{B-1} d\hat{x}_j m_B((\Sigma_{l_i})^2, \mathbf{R}_{l_i}, \hat{\mathbf{x}}_i) \quad (20)$$

$$z((\Sigma_l)^2, \mathbf{R}_l) = z((\Sigma_{l_i})^2, \mathbf{R}_{l_i}) = \int d\hat{\mathbf{x}}_l P_0^l(\hat{\mathbf{x}}_l) e^{-([\hat{\mathbf{x}}_l - \mathbf{R}_l]^2)^T (2\Sigma_l^2)^{-1}} \quad (21)$$

$$\mathbf{f}_{a_i}(\Sigma_{l_i}^2, \mathbf{R}_{l_i}) := \left\{ f_{a_i}(\Sigma_{l_i}^2, \mathbf{R}_{l_i}) := \int d\hat{x}_i m_1((\Sigma_{l_i})^2, \mathbf{R}_{l_i}, \hat{x}_i) \hat{x}_i : i \in \mathbf{l} \right\} \quad (22)$$

$$\mathbf{f}_{c_i}(\Sigma_{l_i}^2, \mathbf{R}_{l_i}) := \left\{ f_{c_i}(\Sigma_{l_i}^2, \mathbf{R}_{l_i}) := \int d\hat{x}_i m_1((\Sigma_{l_i})^2, \mathbf{R}_{l_i}, \hat{x}_i) \hat{x}_i^2 - f_{a_i}(\Sigma_{l_i}^2, \mathbf{R}_{l_i})^2 : i \in \mathbf{l} \right\} \quad (23)$$

We get the second order BP iterations:

$$\mathbf{a}_{l\mu} = \mathbf{f}_{a_l} \left(\frac{1}{\sum_{\gamma \neq \mu}^{M-1} \mathbf{A}_{\gamma l}}, \frac{\sum_{\gamma \neq \mu}^{M-1} \mathbf{B}_{\gamma l}}{\sum_{\gamma \neq \mu}^{M-1} \mathbf{A}_{\gamma l}} \right), \quad \mathbf{v}_{l\mu} = \mathbf{f}_{c_l} \left(\frac{1}{\sum_{\gamma \neq \mu}^{M-1} \mathbf{A}_{\gamma l}}, \frac{\sum_{\gamma \neq \mu}^{M-1} \mathbf{B}_{\gamma l}}{\sum_{\gamma \neq \mu}^{M-1} \mathbf{A}_{\gamma l}} \right) \quad (24)$$

$$\mathbf{a}_\mu = \mathbf{f}_{a_\mu} \left(\frac{1}{\sum_\mu^M \mathbf{A}_{\mu l}}, \frac{\sum_\mu^M \mathbf{B}_{\mu l}}{\sum_\mu^M \mathbf{A}_{\mu l}} \right), \quad \mathbf{v}_\mu = \mathbf{f}_{c_\mu} \left(\frac{1}{\sum_\mu^M \mathbf{A}_{\mu l}}, \frac{\sum_\mu^M \mathbf{B}_{\mu l}}{\sum_\mu^M \mathbf{A}_{\mu l}} \right) \quad (25)$$

At this stage, after indexing with the time, the algorithm defined by the set of equations (17), (24) together with the definitions (20), (22) and (23) is usually referred to as relaxed-BP [11], which is exact in the compressed sensing setting as the number of sections $L \rightarrow \infty$. After convergence, the final estimates are obtained through (25).

We can simplify further the equations, going from an algorithm where $2MN$ messages are exchanged to one where only $M + N$ messages are exchanged. The following expansion is called the Thouless-Anderson-Palmer (TAP) approximation in statistical physics, which is exact in the large signal size limit. It starts by noticing that in the $L \rightarrow \infty$ limit (and thus the number M of factors diverges as well), the cavity quantities (17), (24) become almost independent of the μ index (which is equivalent to saying that each factor's influence becomes infinitely weak). We can thus rewrite these objects as marginal quantities (that depend on single variable indices) keeping the proper first order correction in $F_{\mu i}$. This correcting term called the Onsager reaction term in statistical physics is essential for the efficiency of the AMP algorithm and makes the overall difference with a naive mean-field approach.

We first define new quantities (again, all the operations such as $\frac{1}{\bullet}$ or the dot product $\mathbf{A}\mathbf{B}$ applied to vectors are elementwise, as opposed to $\mathbf{A}^T\mathbf{B}$ which is the usual scalar product between vectors) where \bullet^T is the transpose operator:

$$w_\mu := \sum_k^L \mathbf{F}_{\mu k}^T \mathbf{a}_{k\mu}, \quad \Theta_\mu := \sum_k^L (\mathbf{F}_{\mu k}^2)^T \mathbf{v}_{k\mu} \quad (26)$$

$$\Sigma_k^2 := \frac{1}{\sum_\mu^M \mathbf{A}_{\mu k}}, \quad \mathbf{R}_k := \frac{\sum_\mu^M \mathbf{B}_{\mu k}}{\sum_\mu^M \mathbf{A}_{\mu k}} \quad (27)$$

$$\Sigma_{k\mu}^2 := \frac{1}{\sum_{\gamma \neq \mu}^{M-1} \mathbf{A}_{\gamma k}}, \quad \mathbf{R}_{k\mu} := \frac{\sum_{\gamma \neq \mu}^{M-1} \mathbf{B}_{\gamma k}}{\sum_{\gamma \neq \mu}^{M-1} \mathbf{A}_{\gamma k}} \quad (28)$$

We always remain in the limit $B \in O(1)$ for the derivation, so if B terms $\in O(1/\sqrt{L})$ are summed, the result is still $\in O(1/\sqrt{L})$. In the following, we will need the corrections to the average and variance, so we start by computing them:

$$\mathbf{a}_{l\mu} = \mathbf{f}_{a_l}(\Sigma_{l\mu}^2, \mathbf{R}_{l\mu}) \approx \mathbf{f}_{a_l}(\Sigma_l^2, \mathbf{R}_l) + (\Sigma_{l\mu}^2 - \Sigma_l^2) \nabla_{\Sigma_l^2} \mathbf{f}_{a_l}(\Sigma_l^2, \mathbf{R}_l) + (\mathbf{R}_{l\mu}^2 - \mathbf{R}_l^2) \nabla_{\mathbf{R}_l} \mathbf{f}_{a_l}(\Sigma_l^2, \mathbf{R}_l) \quad (29)$$

$$= \mathbf{a}_l + \left[\frac{\mathbf{A}_{\mu l}}{(\sum_\gamma^M \mathbf{A}_{\gamma l})(\sum_\gamma^M \mathbf{A}_{\gamma l} - \mathbf{A}_{\mu l})} \right] \nabla_{\Sigma_l^2} \mathbf{f}_{a_l}(\Sigma_l^2, \mathbf{R}_l) + \left[\frac{\mathbf{B}_{\mu l}(\sum_\gamma^M \mathbf{A}_{\gamma l}) - \mathbf{A}_{\mu l}(\sum_\gamma^M \mathbf{B}_{\gamma l})}{(\sum_\gamma^M \mathbf{A}_{\gamma l})(\sum_\gamma^M \mathbf{A}_{\gamma l} - \mathbf{A}_{\mu l})} \right] \nabla_{\mathbf{R}_l} \mathbf{f}_{a_l}(\Sigma_l^2, \mathbf{R}_l) \quad (30)$$

Now we use the fact that the $\mathbf{A}_{\gamma l} \in O(1/L)$ is a strictly positive term and $\mathbf{B}_{\gamma l} \in O(1/\sqrt{L})$ can be of both signs thus $\sum_\gamma \mathbf{A}_{\gamma l}$ and $\sum_\gamma \mathbf{B}_{\gamma l}$ are both $\in O(1)$. We obtain, the first order corrections to \mathbf{a}_l and \mathbf{v}_l (following the same computation):

$$\mathbf{a}_{l\mu} = \mathbf{a}_l - \underbrace{\Sigma_l^2 \mathbf{B}_{\mu l} \nabla_{\mathbf{R}_l} \mathbf{f}_{a_l}(\Sigma_l^2, \mathbf{R}_l)}_{\epsilon_{\mathbf{a}_{l\mu}} \in O(1/\sqrt{L})}, \quad \mathbf{v}_{l\mu} = \mathbf{v}_l - \underbrace{\Sigma_l^2 \mathbf{B}_{\mu l} \nabla_{\mathbf{R}_l} \mathbf{f}_{c_l}(\Sigma_l^2, \mathbf{R}_l)}_{\epsilon_{\mathbf{v}_{l\mu}} \in O(1/\sqrt{L})} \quad (31)$$

$\epsilon_{\mathbf{a}_{l\mu}/\mathbf{v}_{l\mu}} := \{\epsilon_{a_{i\mu}/v_{i\mu}} : i \in \mathbf{I}\}$ is the (positive or negative) vector of corrections $\in O(1/\sqrt{L})$ linking $\mathbf{a}_{l\mu}/\mathbf{v}_{l\mu}$ to $\mathbf{a}_l/\mathbf{v}_l$. Expanding the different quantities and keeping only the $O(1)$ terms, we get:

$$\Sigma_l^2 = \left[\sum_\mu^M \frac{\mathbf{F}_{\mu l}}{1/\text{snr} + \Theta_\mu - \mathbf{v}_{l\mu}^T \mathbf{F}_{\mu l}} \right]^{-1} \approx \left[\sum_\mu^M \frac{\mathbf{F}_{\mu l}}{1/\text{snr} + \Theta_\mu} \right]^{-1} \quad (32)$$

$$\mathbf{R}_l = \Sigma_l^2 \left[\sum_\mu^M \frac{\mathbf{F}_{\mu l}(y_\mu - w_\mu + \mathbf{F}_{\mu l} \mathbf{a}_{l\mu}^T)}{1/\text{snr} + \Theta_\mu - \mathbf{v}_{l\mu}^T \mathbf{F}_{\mu l}} \right] \quad (33)$$

$$\approx \Sigma_l^2 \left[\sum_\mu^M \frac{\mathbf{F}_{\mu l}(y_\mu - w_\mu)}{1/\text{snr} + \Theta_\mu} + \underbrace{\sum_\mu^M \mathbf{F}_{\mu l} \frac{(\mathbf{F}_{\mu l})^T \mathbf{a}_l}{1/\text{snr} + \Theta_\mu}}_{\Sigma_l^{-2} \mathbf{a}_l + O(1/\sqrt{L})} - \underbrace{\sum_\mu^M \mathbf{F}_{\mu l} \frac{(\mathbf{F}_{\mu l})^T \epsilon_{\mathbf{a}_{l\mu}}}{1/\text{snr} + \Theta_\mu}}_{\in O(1/L)} \right] \quad (34)$$

$$\approx \mathbf{a}_l + \Sigma_l^2 \sum_\mu^M \frac{\mathbf{F}_{\mu l}(y_\mu - w_\mu)}{1/\text{snr} + \Theta_\mu} \quad (35)$$

$$\Theta_\mu = \sum_k^L (\mathbf{F}_{\mu k}^2)^T \mathbf{v}_k - \underbrace{\sum_k^L (\mathbf{F}_{\mu k}^2)^T \epsilon_{\mathbf{v}_{k\mu}}}_{\in O(1/L)} \approx \sum_k^L (\mathbf{F}_{\mu k}^2)^T \mathbf{v}_k \quad (36)$$

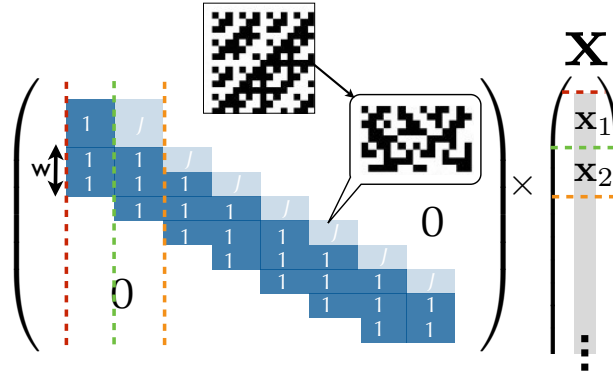


Fig. 5. Representation of the spatially coupled Hadamard sensing operator used in our study. The operator is decomposed in $L_r \times L_c$ blocks, each being made of N/L_c columns and $\alpha_{\text{seed}} N/L_c$ lines for the blocks of the first block-row, $\alpha_{\text{rest}} N/L_c$ lines for the following block-rows (these follow from the definition of $\alpha := M/N$ combined with (1)), with $\alpha_{\text{seed}} > \alpha_{\text{rest}}$. The figure shows how the lines of the original Hadamard matrix (of size $N/L_c \times N/L_c$) are randomly selected, re-ordered and sign-flipped to form a given block of the final operator. There is a number w (the coupling window) of lower diagonal blocks with elements $\in \{\pm 1\}$ as the diagonal blocks, the upper diagonal blocks have elements $\in \{\pm \sqrt{J}\}$ where \sqrt{J} is the coupling strength, all the other blocks contain only zeros. The colored dotted lines help to visualize the block decomposition of the signal induced by the operator structure: each block of the signal will be reconstructed at different times in the algorithm (see Fig. 4 of [19]). The parameters that define the spatially coupled operator ensemble are $(L_c, L_r, w, \sqrt{J}, \alpha_{\text{seed}}, \alpha_{\text{rest}})$. In the paper, the matrix elements are rescaled by $1/\sqrt{L}$ such that the variances are rescaled by $1/L$.

$$w_\mu = \sum_k^L \mathbf{F}_{\mu k}^T \mathbf{a}_k - \sum_k^L \mathbf{F}_{\mu k}^T \boldsymbol{\epsilon}_{\mathbf{a}_{k\mu}} \approx \sum_k^L \mathbf{F}_{\mu k}^T \mathbf{a}_k - \frac{y_\mu - w_\mu}{1/\text{snr} + \Theta_\mu} \sum_k^L (\mathbf{F}_{\mu k}^2)^T \mathbf{v}_k \quad (37)$$

The last equality is obtained neglecting $o(1)$ terms and noticing that:

$$f_{c_i}(\boldsymbol{\Sigma}_{l_i}^2, \mathbf{R}_{l_i}) = v_i = \Sigma_i^2 \partial_{R_i} f_{a_i}(\boldsymbol{\Sigma}_{l_i}^2, \mathbf{R}_{l_i}) \rightarrow \mathbf{f}_{c_l}(\boldsymbol{\Sigma}_l^2, \mathbf{R}_l) = \mathbf{v}_l = \boldsymbol{\Sigma}_l^2 \nabla_{\mathbf{R}_l} \mathbf{f}_{a_l}(\boldsymbol{\Sigma}_l^2, \mathbf{R}_l) \quad (38)$$

combined with (31) and (17). Adding the time indices and rewriting the previous set of equations in terms of their single components, we get the AMP algorithm, see Fig. 4.

The only problem-dependent objects in the AMP are the denoising functions $\{f_{a_i}, f_{c_i}\}$ that depend on the assumed prior. Let us derive them for any power allocation $\{c_l > 0 : l \in \{1, \dots, B\}\}$. The expressions are given by (22) and (23) where here the prior that matches the signal distribution by enforcing the constraint of having only one value $c_l > 0$ per section is:

$$P_0^l(\hat{\mathbf{x}}_l) := \frac{1}{B} \sum_{i \in \mathbb{I}} \delta(\hat{x}_i - c_l) \prod_{j \in \mathbb{I}: j \neq i}^{B-1} \delta(\hat{x}_j) \quad (39)$$

The normalization is:

$$z(\boldsymbol{\Sigma}_l^2, \mathbf{R}_l) = \frac{1}{B} \sum_{i \in \mathbb{I}} \left[e^{-\frac{(c_l - R_i)^2}{2\Sigma_i^2}} \prod_{j \in \mathbb{I}: j \neq i}^{B-1} e^{-\frac{R_j^2}{2\Sigma_j^2}} \right] \quad (40)$$

This matching condition (also called Nishimori condition in statistical physics [12, 30]) allows for great simplifications in the algorithm analysis. Marginalizing over $\{\hat{x}_j \neq \hat{x}_i : j \in \mathbb{I}\}$ we get after simplification the posterior average a_i^t and variance v_i^t of \hat{x}_i at step t of the algorithm:

$$a_i^t := f_{a_i}((\boldsymbol{\Sigma}_{l_i}^t)^2, \mathbf{R}_{l_i}^t) = c_{l_i} \frac{e^{-\frac{c_{l_i}(c_{l_i} - 2R_i^t)}{2(\Sigma_i^t)^2}}}{\sum_{j \in \mathbb{I}}^B e^{-\frac{c_{l_i}(c_{l_i} - 2R_j^t)}{2(\Sigma_j^t)^2}}} \quad (41)$$

$$v_i^t := f_{c_i}((\boldsymbol{\Sigma}_{l_i}^t)^2, \mathbf{R}_{l_i}^t) = a_i^t (c_{l_i} - a_i^t) \quad (42)$$

where $\boldsymbol{\Sigma}_{l_i}, \mathbf{R}_{l_i}$ are the vectors of likelihood standard deviations and means of the components of the section l_i to which the i^{th} component of the signal belongs to. These are sometimes call the ‘‘AMP fields’’ because they are mean fields that summarize the overall influence of the other variables on the i^{th} component. We thus get the full AMP algorithm for sparse superposition codes.

B. The fast Hadamard-based sensing operator

In the present work, we study spatially coupled operator constructed as in Fig. 5: The operator has a block structure with $L_r \times L_c$ blocks, each block being either only zeros or a given matrix such as different random selections of modes of an Hadamard operator (the operator predominantly used in this paper) or a Gaussian i.i.d matrix for example. In the case of an

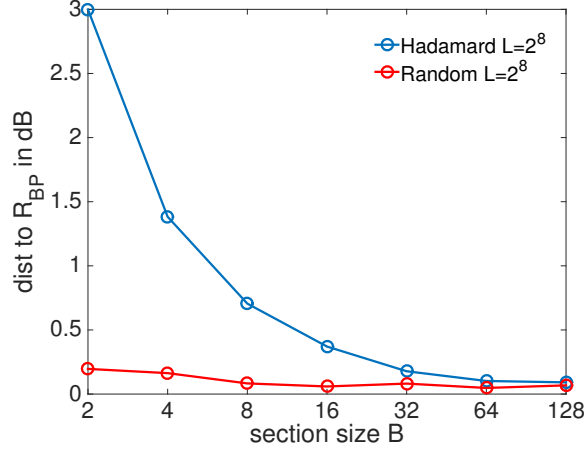


Fig. 6. Comparison between the distance in dB to the asymptotic BP threshold R_{BP} at which the AMP decoder with full Hadamard structured coding operators (blue line) or with random i.i.d Gaussian matrices (red line) starts to reach an SER $< 10^{-5}$ (which is then almost always strictly 0) for a fixed number of sections $L = 2^8$ and snr = 100. The points have been obtained by averaging over 100 random instances. The BP threshold is obtained by state evolution analysis. The Hadamard operator works poorly when the signal density increases (i.e when B decreases), but gets quickly closer to the random matrix performances as it decreases. The random Gaussian i.i.d matrices have a performance that is close to constant as a function of B at fixed L .

Hadamard operator, all the blocks are constructed from the same original Hadamard operator of size $N/L_c \times N/L_c$ with the constraint that N/L_c must be a power of two, intrinsic to the Hadamard construction. The difference between the blocks is the selected modes, their order and the sign of the modes which is randomly flipped.

We define \mathbf{e}_c , with $c \in \{1, \dots, L_c\}$, a vector of size N/L_c , as the c^{th} block of \mathbf{e} (of size N) and \mathbf{f}_r , with $r \in \{1, \dots, L_r\}$, a vector of size $\alpha_r N/L_c$ as the r^{th} block of \mathbf{f} (of size M). For example, in Fig. 5, the signal \mathbf{x} is decomposed as $[\mathbf{x}_1, \dots, \mathbf{x}_{L_c}]$. The notation $i \in \mathbf{c}$ (resp. $\mu \in \mathbf{r}$) means all the components of \mathbf{e} that are in \mathbf{e}_c (resp. all the components of \mathbf{f} that are in \mathbf{f}_r). The algorithm requires four different operators performing the following operations:

$$\tilde{O}_\mu(\mathbf{e}_c) := \sum_{i \in \mathbf{c}}^{N/L_c} F_{\mu i}^2 e_i, \quad O_\mu(\mathbf{e}_c) := \sum_{i \in \mathbf{c}}^{N/L_c} F_{\mu i} e_i \quad (43)$$

$$\tilde{O}_i(\mathbf{f}_r) := \sum_{\mu \in \mathbf{r}}^{\alpha_r N/L_c} F_{\mu i}^2 f_\mu, \quad O_i(\mathbf{f}_r) := \sum_{\mu \in \mathbf{r}}^{\alpha_r N/L_c} F_{\mu i} f_\mu \quad (44)$$

α_r is the measurement rate of all the blocks at the r^{th} block-row, for example on Fig. 5, $\alpha_1 = \alpha_{\text{seed}}$ and $\alpha_j = \alpha_{\text{rest}} \forall j > 1$. Because the value of $F_{\mu i}^2 = 1$ or $J \forall (\mu, i)$ as we use Hadamard operators (it can be read on Fig. 5), all these operators do not require matrix multiplications as they are implemented as fast transforms ($O_\mu()$ and $O_i()$) or simple sums ($\tilde{O}_\mu()$ and $\tilde{O}_i()$). It results in the AMP procedure, see Fig. 4 [19, 31].

In this construction, the link between the overall measurement rate α defined in (1), that of the seed (the first block on the left upper corner on Fig. 5) α_{seed} and that of the bulk α_{rest} is given by:

$$\alpha_{\text{rest}} = \frac{\alpha L_c - \alpha_{\text{seed}}}{L_r - 1} = \alpha \left(\frac{L_c - \beta_{\text{seed}}}{L_r - 1} \right) \quad (45)$$

In practice, α is fixed by choosing the rate R thanks to (1) and $\alpha_{\text{seed}} := \alpha \beta_{\text{seed}}$ as well as by fixing β_{seed} . α_{rest} is then deduced from (45). In the rest of the paper, we will define the spatially coupled ensemble by $(L_c, L_r, w, \sqrt{J}, R, \beta_{\text{seed}})$ instead of $(L_c, L_r, w, \sqrt{J}, \alpha_{\text{seed}}, \alpha_{\text{rest}})$. The physics behind spatial coupling is discussed in more details in Sec. V.

The practical implementation of this operator requires caution: the necessary ‘‘structure killing’’ randomization is obtained by applying a permutation of lines after the use of the fast operator. For each block (r, c) , we choose a random subset of modes $\Omega^{r,c} = \{\Omega_1^{r,c}, \dots, \Omega_{N/L_c}^{r,c}\} \subset \{1, \dots, N/L_c\}$. The definition of $O_\mu(\mathbf{e}_c)$ using a standard fast Hadamard transform \mathbf{H} will be:

$$O_\mu(\mathbf{e}_c) := \mathbf{H}(\mathbf{e}_c) \Big|_{\Omega_{\mu - \mu_{r_\mu} + 1}^{r_\mu, c}} \quad (46)$$

where r_μ is the index of the block row that includes μ , μ_{r_μ} is the number of the first line of the block row r_μ and $\lambda \Big|_\mu$ is the μ^{th} component of λ . For $O_i(\mathbf{f}_r)$ instead,

$$O_i(\mathbf{f}_r) := \mathbf{H}^{-1}(\tilde{\mathbf{f}}_r) \Big|_{i - i_{c_i} + 1} \quad (47)$$

```

1:  $t \leftarrow 0$ 
2:  $\delta \leftarrow \epsilon + 1$ 
3: while  $t < t_{Max}$  and  $\delta > \epsilon$  do
4:    $\Theta_r^{t+1} \leftarrow \sum_c^{L_c} \tilde{O}_r(\mathbf{v}_c^t)$ 
5:    $w_\mu^{t+1} \leftarrow \sum_c^{L_c} O_\mu(\mathbf{a}_c^t) - \Theta_{r_\mu}^{t+1} \frac{y_\mu - w_\mu^t}{1/\text{snr} + \Theta_{r_\mu}^t}$ 
6:    $\Sigma_c^{t+1} \leftarrow \left[ \sum_r^{L_r} \tilde{O}_c \left( [1/\text{snr} + \Theta_r^{t+1}]^{-1} \right) \right]^{-1/2}$ 
7:    $R_i^{t+1} \leftarrow a_i^t + (\Sigma_{c_i}^{t+1})^2 \sum_r^{L_r} O_i \left( \frac{\mathbf{y}_r - \mathbf{w}_r^{t+1}}{1/\text{snr} + \Theta_r^{t+1}} \right)$ 
8:    $v_i^{t+1} \leftarrow f_{c_i} \left( (\Sigma_{c_i}^{t+1})^2, \mathbf{R}_{l_i}^{t+1} \right)$ 
9:    $a_i^{t+1} \leftarrow f_{a_i} \left( (\Sigma_{c_i}^{t+1})^2, \mathbf{R}_{l_i}^{t+1} \right)$ 
10:   $t \leftarrow t + 1$ 
11:   $\delta \leftarrow 1/N \sum_i^N (a_i^t - a_i^{t-1})^2$ 
12: end while
13: return  $\{a_i\}$ 

```

Fig. 7. The simplified (with respect to Fig. 4) AMP decoder for sparse superposition codes, where we have approximated the squared elements of the matrix by their variance.

where c_i is the index of the block column that includes i , i_{c_i} is the number of the first column of the block column c_i , \mathbf{H}^{-1} is the standard Hadamard fast inverse operator of \mathbf{H} (which is actually \mathbf{H} itself) and $\tilde{\mathbf{f}}_r$ is defined in the following way:

$$\forall \gamma \in \{1, \dots, N/L_r\}, \quad \tilde{\mathbf{f}}_r |_{\Omega_r^{\gamma,c}} = \mathbf{f}_r |_\gamma \quad \text{and} \quad \forall i \notin \Omega_r^{\gamma,c}, \quad \tilde{\mathbf{f}}_r |_i = 0. \quad (48)$$

Fig. 6 shows that when the signal sparsity increases, i.e. when the section size B increases, using Hadamard based operators becomes equivalent to random i.i.d Gaussian ones in terms of performances (this point is studied in more details in [19]). We fix the $\text{snr} = 100$ and plot the distance in dB to the BP threshold R_{BP} (defined as the highest rate until which AMP decoding is optimal without the need of non constant power allocation or spatial coupling) at which the decoder starts to decode perfectly with Hadamard or random Gaussian operators. It appears that at low section size, it is advantageous to use random operators but as B increases, structured operators quickly reach the random operator performances. The BP threshold is predicted by the state evolution analysis presented in Sec. IV.

C. Further simplifications for random matrices with zero mean

We can go further in the approximation of some quantities computed in the decoder Fig. 4 by considering the elements $F_{\mu i}^2$ equal to their variance $F_{\mu i}^2 = J_{r_\mu, c_i}/L$. This is justified by the fact that the average with respect to the matrix realization of all the objects appearing in the decoder depending on such squared elements (such as Θ_μ) are $\in O(1)$ whilst their variance $\in O(1/N)$, see [12]. Thus in the large signal limit, we can neglect their fluctuations by simply replacing the matrix squared elements by their variance. Considering the most general version of AMP (the left version of Fig. 4) where it is written in terms of the operators, the dependency is just in the $\tilde{O}_\mu(\cdot)$ and $\tilde{O}_i(\cdot)$ operators that now depend only on the block indices and can thus be approximated as:

$$\tilde{O}_r(\mathbf{e}_c) := \frac{J_{r,c}}{L} \sum_{i \in \mathbf{c}} e_i, \quad \tilde{O}_c(\mathbf{f}_r) := \frac{J_{r,c}}{L} \sum_{\mu \in \mathbf{r}} \alpha_r N/L_c f_\mu \quad (49)$$

Now we show how to go from this simplified form of the AMP decoder Fig. 7 to the notation of [15] in the case of a full matrix. Starting from Fig. 7, we plug the R_i^{t+1} expression into the denoising function defining the residual $\boldsymbol{\tau}_r^t := \{\tau_\mu^t : \mu \in \mathbf{r}\}$ and using the iteration of \mathbf{w}_r^{t+1} :

$$a_i^{t+1} = f_{a_i} \left((\Sigma_{c_i}^{t+1})^2, \underbrace{\left\{ a_j^t + (\Sigma_{c_i}^{t+1})^2 \sum_r^{L_r} O_i \left(\frac{\tau_r^t}{1/\text{snr} + \Theta_r^{t+1}} \right) : j \in \mathbf{l}_i \right\}}_{:= \mathbf{R}_{l_i}^{t+1}} \right) \quad (50)$$

$$\boldsymbol{\tau}_r^t := \mathbf{y}_r - \mathbf{w}_r^{t+1} = \mathbf{y}_r - \left\{ \sum_c^{L_c} O_\mu(\mathbf{a}_c^t) : \mu \in \mathbf{r} \right\} + \Theta_r^{t+1} \frac{\mathbf{y}_r - \mathbf{w}_r^t}{1/\text{snr} + \Theta_r^t} \quad (51)$$

$$= \mathbf{y}_r - \left\{ \sum_c^{L_c} O_\mu(\mathbf{a}_c^t) : \mu \in \mathbf{r} \right\} + \tau_r^{t-1} \frac{\Theta_r^{t+1}}{1/\text{snr} + \Theta_r^t} \quad (52)$$

where we considered that we have defined the groups such that all the 1-d components inside the same section are of course in the same group. Now using the definition of $\Theta_r^{t+1} =: \mathbf{1}_{\alpha_r N/L_c} \Theta_r^{t+1}$ we obtain:

$$\Theta_r^{t+1} = \frac{B}{L_c} \sum_c^{L_c} J_{r,c} \langle f_c^t \rangle_c = \frac{B}{L_c} \sum_c^{L_c} J_{r,c} (\Sigma_c^t)^2 \langle (f_a^t)' \rangle_c \quad (53)$$

where we have used the property (38) of the denoising function for the last equality and we used the shorthand notations:

$$\langle f_c^t \rangle_c := \frac{L_c}{N} \sum_{i \in \mathbf{c}}^{N/L_c} f_{c_i}((\Sigma_c^t)^2, \mathbf{R}_{i_c}^t), \quad \langle (f_a^t)' \rangle_c := \frac{L_c}{N} \sum_{i \in \mathbf{c}}^{N/L_c} \left(\frac{\partial f_{a_i}(x, \mathbf{y})}{\partial y_i} \right)_{(\Sigma_c^t)^2, \mathbf{R}_{i_c}^t} \quad (54)$$

It closes the equations. Let us show that this form gives back the usual one in the full operator case ($L_c = L_r = J_{r,c} = 1$). In this case, the quantities in the algorithm become:

$$\Theta^{t+1} = B(\Sigma^t)^2 \langle (f_a^t)' \rangle \quad (55)$$

$$(\Sigma^{t+1})^2 = (\Theta^{t+1} + 1/\text{snr})/(B\alpha) \quad (56)$$

$$(57)$$

$$\rightarrow a_i^{t+1} = f_{a_i} \left((\Sigma^{t+1})^2, \left\{ a_j^t + (\Sigma^{t+1})^2 \sum_{\mu}^M F_{\mu j} \tau_{\mu}^t \frac{1}{\Theta^{t+1} + 1/\text{snr}} : j \in \mathbf{I}_i \right\} \right) \quad (58)$$

$$= f_{a_i} \left((\Sigma^{t+1})^2, \left\{ a_j^t + 1/(B\alpha) \sum_{\mu}^M F_{\mu j} \tau_{\mu}^t : j \in \mathbf{I}_i \right\} \right) \quad (59)$$

$$\rightarrow \tau_{\mu}^t = y_{\mu} - \sum_i^N F_{\mu i} a_i^t + \tau_{\mu}^{t-1} \frac{\Theta^{t+1}}{1/\text{snr} + \Theta^t} = y_{\mu} - \sum_i^N F_{\mu i} a_i^t + \tau_{\mu}^{t-1} \frac{B(\Sigma^t)^2 \langle (f_a^t)' \rangle}{B\alpha(\Sigma^t)^2} \quad (60)$$

$$= y_{\mu} - \sum_i^N F_{\mu i} a_i^t + \tau_{\mu}^{t-1} \frac{\langle (f_a^t)' \rangle}{\alpha} \quad (61)$$

The last step is to rescale the coding matrix by dividing its elements by $B\alpha : \tilde{\mathbf{F}} := \mathbf{F}/(B\alpha)$. The measure $\tilde{\mathbf{y}}$ is thus rescaled in the same way. We finally obtain the more classical form of AMP for homogeneous matrices:

$$\tilde{\tau}_{\mu}^t = \tilde{y}_{\mu} - \sum_i^N \tilde{F}_{\mu i} a_i^t + \tilde{\tau}_{\mu}^{t-1} \langle (f_a^t)' \rangle / \alpha \quad (62)$$

$$(\Sigma^{t+1})^2 = ((\Sigma^t)^2 \langle (f_a^t)' \rangle + 1/(B\text{snr})) / \alpha \quad (63)$$

$$a_i^{t+1} = f_{a_i} \left((\Sigma^{t+1})^2, \left\{ a_j^t + \sum_{\mu}^M \tilde{F}_{\mu j} \tilde{\tau}_{\mu}^t : j \in \mathbf{I}_i \right\} \right) \quad (64)$$

where $\tilde{\tau}^t$ is the rescaled residual, and:

$$\langle (f_a^t)' \rangle := \frac{1}{N} \sum_i^N \left(\frac{\partial f_{a_i}(x, \mathbf{y})}{\partial y_i} \right)_{(\Sigma^t)^2, \{a_j^{t-1} + \sum_{\mu}^M \tilde{F}_{\mu j} \tilde{\tau}_{\mu}^{t-1} : j \in \mathbf{I}_i\}} \quad (65)$$

$$= \frac{1}{N(\Sigma^t)^2} \sum_i^N f_{c_i} \left((\Sigma^t)^2, \left\{ a_j^{t-1} + \sum_{\mu}^M \tilde{F}_{\mu j} \tilde{\tau}_{\mu}^{t-1} : j \in \mathbf{I}_i \right\} \right) \quad (66)$$

IV. STATE EVOLUTION ANALYSIS FOR RANDOM I.I.D DENSE OPERATORS WITH CONSTANT POWER ALLOCATION

The state evolution technique (referred to as the cavity method in physics) is a statistical analysis [16] that allows to monitor the AMP dynamics and performance in the limit of decoding infinitely large signals. We consider here the case of i.i.d Gaussian elements for the matrix \mathbf{F} for which state evolution has been originally derived. Extension to more general ensembles such as row orthogonal matrices could be considered [32] but it is out of the scope of the present paper. In addition, the present authors have numerically shown in [19] that the state evolution analysis derived in the random i.i.d case is a good predictive tool of the behavior of the AMP decoder with structured operators, despite not perfect nor rigorous.

We assume the proper scaling to get a codeword with power $P = 1$: $F_{ij} \in O(1/\sqrt{L}) \forall (i, j)$. For the moment, we consider the case of a constant power allocation $\{c_l = 1 \forall l \in \{1, \dots, L\}\}$ which drastically simplifies the analysis due to the symmetry between all the sections. We will look at the more general case in the next section. One can perform the analysis starting

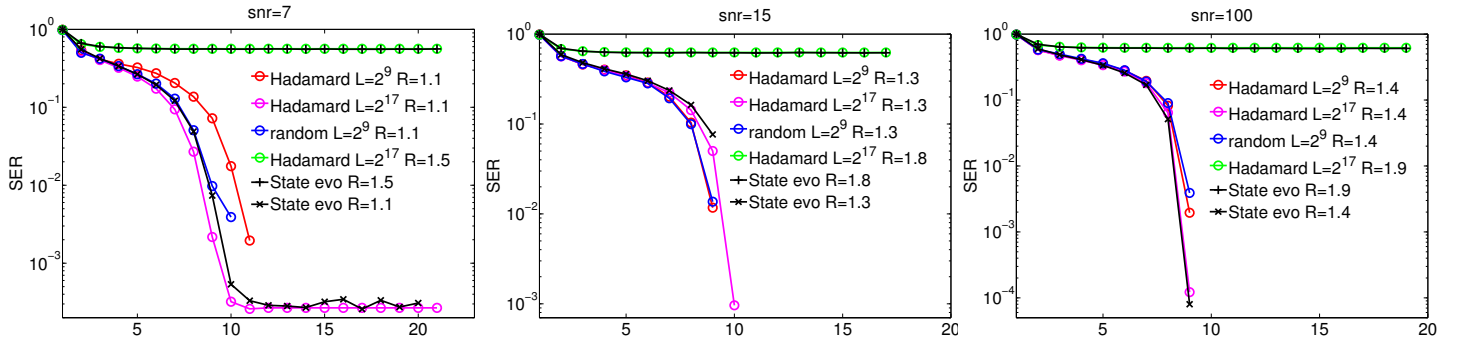


Fig. 8. The state evolution prediction of the section error rate SER^t as a function of time (black curves), compared to the actual SER^t of the AMP decoder for $\text{snr} = 7/15/100$, different rates R (one above and one below the BP threshold R_{BP}), a section size $B=64$, different signal size L values and in the full Hadamard based or purely random i.i.d Gaussian operator case with constant power allocation $\{c_l = 1 \forall l \in \{1, \dots, L\}\}$. The state evolution is computed by monte carlo technique with a sample size of 10^6 . The figure shows how close is the prediction from the true behavior for finite sizes. For high snr, the finite size curves stop without reaching a threshold because the recovery is actually perfect and the final $\text{SER} = 0$ which is due to the finite size effects. The same happens for the theoretical curves that reach 0 due to finite numerical precision. We observe that when the signal size L is big (and thus that we must use the Hadamard operator because of speed and memory issues), the algorithm behavior follows the theoretical predictions very closely.

from the cavity quantities defined in the previous section as in [12], but here we will follow another path starting from the algorithm itself Fig.4.

The aim is to estimate the asymptotic posterior average of a 1-d variable in order to compute the asymptotic biased MSE \tilde{E}^t from which we can deduce the asymptotic SER^t . The posterior average is given by (41) which is a deterministic variable at fixed $(\Sigma_l^t, \mathbf{R}_l^t)$. We thus need to get an estimate of \mathbf{R}_l^t , the average of variable \mathbf{x}_l at time t with respect to the likelihood. Σ_l^t is its associated variance. Injecting the definitions Fig. 4 of the quantities appearing in the \mathbf{R}_l^t term and recalling the definition of $B\alpha := M/L$ and (5), we get the following expression for \mathbf{R}_l^t :

$$\mathbf{R}_l^{t+1} = \mathbf{a}_l^t + (\Sigma_l^{t+1})^2 \sum_{\mu} \frac{\mathbf{F}_{\mu l}}{1/\text{snr} + \Theta_{\mu}^{t+1}} \left[\sum_k \mathbf{F}_{\mu k}^T (\mathbf{x}_k - \mathbf{a}_k^t) + \xi_{\mu} + \underbrace{\Theta_{\mu}^{t+1} \frac{y_{\mu} - w_{\mu}^t}{1/\text{snr} + \Theta_{\mu}^t}}_{:=\Lambda_{\mu}^t} \right] \quad (67)$$

$$\approx \mathbf{x}_l + \frac{1}{B\alpha} \sum_{\mu} \mathbf{F}_{\mu l} \left[\underbrace{\sum_{k \neq l} \mathbf{F}_{\mu k}^T (\mathbf{x}_k - \mathbf{a}_k^t) + \xi_{\mu} + \Lambda_{\mu}^t}_{:=\mathbf{r}_l^{t+1}} \right] \quad (68)$$

where we have used that Θ_{μ}^t is asymptotically independent of μ as we can replace the $F_{\mu i}^2$ elements by the matrix variance $1/L$:

$$\Theta_{\mu}^t \approx \Theta^t := 1/L \sum_i v_i^t \rightarrow (\Sigma_l^{t+1})^2 \approx \frac{1/\text{snr} + \Theta^{t+1}}{B\alpha} \mathbf{1}_B \quad (69)$$

and the fact that we can directly forget about the second part in:

$$\sum_{\mu} \mathbf{F}_{\mu l} \left[\mathbf{F}_{\mu l}^T (\mathbf{x}_l - \mathbf{a}_l^t) \right] = \underbrace{\left\{ \sum_{\mu} F_{\mu i}^2 (x_i - a_i^t) : i \in \mathbf{I} \right\}}_{=B\alpha(\mathbf{x}_l - \mathbf{a}_l^t)} + \underbrace{\left\{ \sum_{\mu} \sum_{j \in \mathbf{I}; j \neq i} F_{\mu i} F_{\mu j} (x_j - a_j^t) : i \in \mathbf{I} \right\}}_{\in O(1/\sqrt{L})} \quad (70)$$

as we will keep only $O(1)$ terms in the computations of the moments of the fluctuations of \mathbf{R}_l^{t+1} around \mathbf{x}_l . $\mathbf{1}_B$ is a vector of ones of size B . Now we notice from (37) that:

$$\Lambda_{\mu}^t \approx \sum_k \mathbf{F}_{\mu k}^T \epsilon_{a_{k\mu}} \quad (71)$$

where $\epsilon_{a_{k\mu}} \in O(1/\sqrt{L})$ is given by (31), (37). Using the independence assumption of the operator \mathbf{F} elements, we can apply the central limit theorem to \mathbf{r}_l^t which is thus Gaussian distributed with moments that we compute now. We remind the reader that the noise has zero mean and we note that the biased MSE (6) becomes in the large size signals limit:

$$\tilde{E}^{t+1} = 1/N \sum_k \mathbb{E}_{\mathbf{F}, \xi, \mathbf{x}} \left\{ [\mathbf{x}_k - \mathbf{a}_k^{t+1}]^T [\mathbf{x}_k - \mathbf{a}_k^{t+1}] \right\} \xrightarrow{L \rightarrow \infty} \mathbb{E}_{\mathbf{F}, \mathbf{x}, \xi} \left\{ [x_j - a_j^{t+1}]^2 \right\} \quad (72)$$

where \mathbf{a}^t is the AMP estimate of the signal at time t as before (41). The matrix \mathbf{F} elements having 0 mean, only the terms with even power of the matrix elements in the various sums that appear remain because of the average so that, using (71), we obtain:

$$\mathbb{E}_{\mathbf{F}, \xi, \mathbf{x}} \{ \mathbf{r}_l^{t+1} \} = \underbrace{\mathbb{E}_{\mathbf{F}, \xi, \mathbf{x}} \left\{ \sum_{\mu}^M \mathbf{F}_{\mu l} \sum_{k \neq l}^{L-1} \mathbf{F}_{\mu k}^T (\mathbf{x}_k - \mathbf{a}_k^t) + \sum_{\mu}^M \mathbf{F}_{\mu l} \xi_{\mu} \right\}}_{=0_B} + \mathbb{E}_{\mathbf{F}, \xi, \mathbf{x}} \left\{ \sum_{\mu}^M \mathbf{F}_{\mu l} \sum_k^L \mathbf{F}_{\mu k}^T \epsilon_{\alpha_{k\mu}} \right\} \quad (73)$$

$$\approx \underbrace{\mathbb{E}_{\mathbf{F}, \xi, \mathbf{x}} \left\{ \sum_{\mu}^M (\mathbf{F}_{\mu l}^3)^T \mathbf{v}_l \frac{y_{\mu} - w_{\mu}^t}{1/\text{snr} + \Theta^t} \right\}}_{\in O(1/L)} \approx \mathbf{0}_B \quad (74)$$

$$\mathbb{E}_{\mathbf{F}, \xi, \mathbf{x}} \{ \mathbf{r}_l^{t+1} \mathbf{r}_{l'}^{t+1} \}_{l' \neq l} = \mathbb{E}_{\mathbf{F}, \xi, \mathbf{x}} \left\{ \sum_{\mu, \nu}^{M, M} \mathbf{F}_{\mu l} \mathbf{F}_{\nu l'} \left[\sum_{k \neq l}^{L-1} \mathbf{F}_{\mu k}^T (\mathbf{x}_k - \mathbf{a}_k^t) + \xi_{\mu} + \Lambda_{\mu}^t \right] \left[\sum_{k' \neq l'}^{L-1} \mathbf{F}_{\nu k'}^T (\mathbf{x}_{k'} - \mathbf{a}_{k'}^t) + \xi_{\nu} + \Lambda_{\nu}^t \right] \right\} \quad (75)$$

$$= \mathbb{E}_{\mathbf{F}, \xi, \mathbf{x}} \left\{ \sum_{\mu}^M \mathbf{F}_{\mu l} \mathbf{F}_{\mu l'} \left[\mathbf{F}_{\mu l'}^T (\mathbf{x}_{l'} - \mathbf{a}_{l'}^t) + \xi_{\mu} + \Lambda_{\mu}^t \right] \left[\mathbf{F}_{\mu l}^T (\mathbf{x}_l - \mathbf{a}_l^t) + \xi_{\mu} + \Lambda_{\mu}^t \right] \right\} \quad (76)$$

$$= \underbrace{\mathbb{E}_{\mathbf{F}, \xi, \mathbf{x}} \left\{ \sum_{\mu}^M \mathbf{F}_{\mu l}^2 \mathbf{F}_{\mu l'}^2 (\mathbf{x}_{l'} - \mathbf{a}_{l'}^t) (\mathbf{x}_l - \mathbf{a}_l^t) \right\}}_{\in O(1/L)} \approx \mathbf{0}_B \quad (77)$$

$$\mathbb{E}_{\mathbf{F}, \xi, \mathbf{x}} \{ (\mathbf{r}_l^{t+1})^2 \} = \mathbb{E}_{\mathbf{F}, \xi, \mathbf{x}} \left\{ \sum_{\mu, \nu}^{M, M} \mathbf{F}_{\mu l} \mathbf{F}_{\nu l} \left[\sum_{k \neq l}^{L-1} \mathbf{F}_{\mu k}^T (\mathbf{x}_k - \mathbf{a}_k^t) + \xi_{\mu} + \Lambda_{\mu}^t \right] \left[\sum_{k' \neq l}^{L-1} \mathbf{F}_{\nu k'}^T (\mathbf{x}_{k'} - \mathbf{a}_{k'}^t) + \xi_{\nu} + \Lambda_{\nu}^t \right] \right\} \quad (78)$$

$$= \mathbb{E}_{\mathbf{F}, \xi, \mathbf{x}} \left\{ \sum_{\mu}^M \mathbf{F}_{\mu l}^2 \left[\sum_{k \neq l}^{L-1} \mathbf{F}_{\mu k}^T (\mathbf{x}_k - \mathbf{a}_k^t) + \xi_{\mu} + \Lambda_{\mu}^t \right] \left[\sum_{k' \neq l}^{L-1} \mathbf{F}_{\mu k'}^T (\mathbf{x}_{k'} - \mathbf{a}_{k'}^t) + \xi_{\mu} + \Lambda_{\mu}^t \right] \right\} \quad (79)$$

$$= \mathbb{E}_{\mathbf{F}, \xi, \mathbf{x}} \left\{ \sum_{\mu}^M \mathbf{F}_{\mu l}^2 \left[\sum_{k \neq l}^{L-1} \mathbf{F}_{\mu k}^T (\mathbf{x}_k - \mathbf{a}_k^t) \right] \left[\sum_{k' \neq l}^{L-1} \mathbf{F}_{\mu k'}^T (\mathbf{x}_{k'} - \mathbf{a}_{k'}^t) \right] \right\} + \frac{\alpha B}{\text{snr}} + \underbrace{\mathbb{E}_{\mathbf{F}, \xi, \mathbf{x}} \left\{ \sum_{\mu}^M \mathbf{F}_{\mu l}^2 \Lambda_{\mu}^2 \right\}}_{\in O(L^{-3/2})} + 2 \underbrace{\mathbb{E}_{\mathbf{F}, \xi, \mathbf{x}} \left\{ \sum_{\mu}^M \mathbf{F}_{\mu l} \Lambda_{\mu} \left[\sum_{k \neq l}^{L-1} \mathbf{F}_{\mu k}^T (\mathbf{x}_k - \mathbf{a}_k^t) \right] \right\}}_{=0_B} \quad (80)$$

$$\approx \mathbb{E}_{\mathbf{F}, \xi, \mathbf{x}} \left\{ \sum_{\mu}^M \mathbf{F}_{\mu l}^2 \left[\sum_{k \neq l}^{L-1} (\mathbf{F}_{\mu k}^2)^T (\mathbf{x}_k - \mathbf{a}_k^t)^2 \right] \right\} + \frac{\alpha B}{\text{snr}} \quad (81)$$

$$\approx \frac{M}{L^2} \sum_k^L \mathbb{E}_{\mathbf{x}} \{ (\mathbf{x}_k - \mathbf{a}_k^t)^T (\mathbf{x}_k - \mathbf{a}_k^t) \} + \frac{\alpha B}{\text{snr}} = B\alpha \left(1/\text{snr} + B\tilde{E}^t \right) \quad (82)$$

where $\mathbf{0}_B$ is a vector of zeros of size B . Let's now write R_i^t as a Gaussian variable:

$$r_i^{t+1} \sim \mathcal{N}_{0, B\alpha(1/\text{snr} + B\tilde{E}^t)} \rightarrow R_i^{t+1} \sim \mathcal{N}_{x_i, \frac{1/(\text{snr}B) + \tilde{E}^t}{\alpha}} \quad (83)$$

It remains to perform the average over the signal \mathbf{x} distribution. We can actually look at the biased MSE in a single section which is the same as the overall one given that the sections are all equivalent, the power allocation being constant. Thus the state evolution in the matching prior case, with knowledge of the channel noise is:

$$\tilde{E}^{t+1} = 1/B \sum_{i \in \mathcal{I}}^B \int d\mathbf{x}_l \mathcal{D}\mathbf{z} P_0(\mathbf{x}_l) \left[f_{a_i} \left((\tilde{\Sigma}^{t+1})^2, \mathbf{R}^{t+1}(\mathbf{z}, \mathbf{x}_l) \right) - x_i \right]^2 \quad (84)$$

$$= 1/B \int \mathcal{D}\mathbf{z} \left[f_{a_1} \left((\tilde{\Sigma}^{t+1})^2, \mathbf{R}^{(1), t+1}(\mathbf{z}) \right) - 1 \right]^2 + (1 - 1/B) \int \mathcal{D}\mathbf{z} f_{a_1} \left((\tilde{\Sigma}^{t+1})^2, \mathbf{R}^{(2), t+1}(\mathbf{z}) \right)^2 \quad (85)$$

where $\mathcal{D}\mathbf{z}$ is a B -d unit centered Gaussian measure and $P_0(\mathbf{x}_l)$ is the prior with constant power allocation:

$$\mathcal{D}\mathbf{z} := \prod_i^B \mathcal{D}z_i = \prod_i^B \mathcal{N}_{0,1}(z_i) dz_i \quad (86)$$

$$P_0(\mathbf{x}_l) := 1/B \sum_{i \in \mathbf{l}} \delta(x_i - 1) \prod_{j \in \mathbf{l}: j \neq i} \delta(x_j) \quad (87)$$

and where f_{a_1} is given by (41) and $\mathbf{R}^{(i),t+1}(\mathbf{z})$ is such that:

$$R_j^{(i),t+1}(\mathbf{z}, \tilde{E}^t) := \delta_{i,j} + z_j \tilde{\Sigma}^{t+1}(\tilde{E}^t), \quad z_j \sim \mathcal{N}_{0,1} \quad \forall j \in \{1, \dots, B\} \quad (88)$$

$$\tilde{\Sigma}^{t+1}(\tilde{E}^t) := \sqrt{(1/(\text{snr}B) + \tilde{E}^t)/\alpha} = \sqrt{\frac{RB(1/(\text{snr}B) + \tilde{E}^t)}{\log_2 B}} \quad (89)$$

where $\delta_{i,j}$ is the kroneker symbol. In the previous equations (84) and (85), the explicit dependency in \tilde{E}^t of $\mathbf{R}^{(i),t+1}(\mathbf{z})$ and $\tilde{\Sigma}^{t+1}$ has been dropped out for clarity but must not be forgotten. We now rewrite it only in terms of rescaled $O(1)$ quantities:

$$E^t := B\tilde{E}^t, \quad \Sigma^{t+1}(E^t) := \tilde{\Sigma}^{t+1}(\tilde{E}^t) \sqrt{\log(B)} = \sqrt{R(1/\text{snr} + E^t) \log(2)} \quad (90)$$

Removing the index i (all the blocks are equivalent from the constant power allocation assumption) and after basic algebraic operations, we get:

$$E^{t+1} = \int \mathcal{D}\mathbf{z} ([f_{a_{1|1}}((\Sigma^{t+1})^2, \mathbf{z}) - 1]^2 + (B-1)f_{a_{2|1}}((\Sigma^{t+1})^2, \mathbf{z})^2) \quad (91)$$

where:

$$f_{a_{i|i}}(\Sigma^2, \mathbf{z}) := \left[1 + e^{-\frac{\log(B)}{\Sigma^2}} \sum_{\{1 \leq j \leq B: j \neq i\}}^{B-1} e^{\frac{\sqrt{\log(B)}(z_j - z_i)}{\Sigma}} \right]^{-1} \quad (92)$$

$$f_{a_{j|i}}(\Sigma^2, \mathbf{z}) := \left[1 + e^{\frac{\log(B)}{\Sigma^2} + \frac{\sqrt{\log(B)}(z_j - z_i)}{\Sigma}} + \sum_{\{1 \leq k \leq B: k \neq i, j\}}^{B-2} e^{\frac{\sqrt{\log(B)}(z_k - z_i)}{\Sigma}} \right]^{-1} \quad (93)$$

In the constant power allocation framework, the quantity $f_{a_{i|i}}$ ($f_{a_{j|i}}$) can be interpreted as the asymptotic posterior probability estimate of the i^{th} component (j^{th} component) to be the 1 component by the AMP algorithm knowing that it is actually the true 1 in the signal (knowing that it is actually the i^{th} that is the true 1). In this approach, there is a one to one correspondance from the value of the biased MSE to the SER thanks to the mapping:

$$\text{SER}^{t+1} = \int \mathcal{D}\mathbf{z} \mathbb{I}(\exists j \in \{2, \dots, B\} : f_{a_{j|1}}((\Sigma^{t+1})^2, \mathbf{z}) > f_{a_{1|1}}((\Sigma^{t+1})^2, \mathbf{z})) \quad (94)$$

From this equation, we can rigorously predict the evolution in time of the algorithm, such as in Fig. 8. The black curves on this plot represent the iteration of (94) for different experimental settings ensembles (snr, R) in the asymptotic limit $L \rightarrow \infty$ and fixed section size $B = 64$ using full randomized Hadamard or purely random Gaussian i.i.d matrices. (94) and (91) are computed at each time step by monte carlo technique. We observe that for the $\text{snr} = 15/100$ cases, the experimental and theoretical curves stop at some iteration without reaching a noise floor. For the experimental curves, this is due to the fact that in order to observe an $\text{SER} \in O(\epsilon)$, there must be at least $L \approx 1/\epsilon$ sections which is not the case for signals of reasonable sizes, when the asymptotic SER is very small. In fact, when the rate is below the threshold, the decoding is usually perfect and is found to reach with high probability $\text{SER}=0$. The black theoretical curves should anyway reach a finite error floor but they do not because this floor is so low that the sample size used in the monte carlo computation could be way too large to deal with by the same argument.

Another observation, natural from the definition of the state evolution technique as an asymptotic analysis, is that the theoretical and experimental results match better for larger signals. At rate $R > R_{BP}$ larger than the BP threshold (green experimental curve and associated theoretical curve), we see that the AMP decoding does not reconstruct the signal and converges to a high SER solution well predicted by the state evolution. On the contrary, below the threshold, the reconstruction works fine up to an error floor dependent on the parameters (B, snr, R). We also observe as in [19] that the state evolution, even if derived for random i.i.d Gaussian matrices, predicts well the behavior of AMP with Hadamard based operators.

The matching prior condition [12] implies another way of expressing the biased MSE that will be useful later on in Sec. VI-B to show the equivalence between the replica and state evolution analysis in an easy manner. The biased MSE can be expressed as:

$$\tilde{E}^{t+1} = \mathbb{E}_{\mathbf{F}, \mathbf{x}, \xi}^{t+1} \{ [x_j - a_j^{t+1}]^2 \} = \mathbb{E}_{\mathbf{x}} \{ x_j^2 \} + \mathbb{E}_{\mathbf{F}, \mathbf{x}, \xi} \{ (a_j^{t+1})^2 \} - 2\mathbb{E}_{\mathbf{F}, \mathbf{x}, \xi} \{ x_j a_j^{t+1} \} = \mathbb{E}_{\mathbf{x}} \{ x_j^2 \} - \mathbb{E}_{\mathbf{F}, \mathbf{x}, \xi} \{ x_j a_j^{t+1} \} \quad (95)$$

where we have used $\mathbb{E}_{\mathbf{F}, \mathbf{x}, \xi} \{(a_j^{t+1})^2\} = \mathbb{E}_{\mathbf{F}, \mathbf{x}, \xi} \{x_j a_j^{t+1}\}$ which is a consequence of the matching prior condition, see [12] for the proof. From the previous derivation, we obtain:

$$E^{t+1} = 1 - \sum_{i \in \mathcal{I}} \int d\mathbf{x}_i \mathcal{D}\mathbf{z} P_0(\mathbf{x}_i) f_{a_i} \left((\tilde{\Sigma}^{t+1})^2, \mathbf{R}^{t+1}(\mathbf{z}, \mathbf{x}_i) \right) x_i \quad (96)$$

$$= 1 - \int \mathcal{D}\mathbf{z} f_{a_{11}} \left((\tilde{\Sigma}^{t+1})^2, \mathbf{R}^{(1), t+1}(\mathbf{z}) \right) = 1 - \int \mathcal{D}\mathbf{z} f_{a_{11}} \left((\Sigma^{t+1})^2, \mathbf{z} \right) \quad (97)$$

where we have used $\mathbb{E}_{\mathbf{x}} \{x_j^2\} = 1/B$ and (90). This equivalent form is computationally easier and faster to deal with but can be more dangerous to use than (91) because it can become negative if the difference is really small due to finite numerical precision.

V. STATE EVOLUTION ANALYSIS FOR SPATIALLY COUPLED I.I.D OPERATORS OR POWER ALLOCATION

Mean-field systems (systems for which mean-field techniques such as message-passing algorithms are appropriate) are of two types: the problems defined on sparse random graphs such as random K-SAT or many other combinatorial optimization problems and problems defined on densely-connected graphs such as in the present case (5). In these homogeneous systems, nucleation (a local change of thermodynamical phase) cannot occur because it is a consequence of the interplay of surface and bulk energy terms and a mean field system is equivalent to an infinite dimensional system, thus the surface term is always infinite. There is no locality in these systems: no nucleus can spread. In inference problems, the phases we are dealing with are referred to easy/hard/impossible inference phases. In order to have nucleation of an easy inference phase inside a hard inference one and to allow this nucleus to propagate inside the full system, one has to introduce a dimensionality, or structure in the problem. This is done by spatial coupling techniques, using a properly designed coding operator, see Fig. 5.

Spatial coupling has been introduced in the context of LDPC codes [9] and has been extensively used in the compressed sensing setting as well [11–14]. It rigorously allows to reach the information theoretical bound in LDPC [9] and in compressed sensing in the random i.i.d measurement matrix case [9, 13]. The decoding part in the sparse superposition codes scheme being a structured compressed sensing problem, spatial coupling works well [11, 12]. In order to get a practical algorithm, able to decode very large signals, we combine spatial coupling techniques with the use of a structured operator, the Hadamard one which has been shown to be as efficient as the purely random coding (or sensing in the compressed sensing context) matrices [19, 33, 34].

The way the operator is constructed is described in Sec. III and Fig. 5. The spatial structure described above is induced in the signal by the block structure of the coding matrix. The signal becomes the concatenation of sub-systems $\mathbf{x} = [\mathbf{x}_1, \dots, \mathbf{x}_{L_c}]$. One has to be careful to ensure that these sub-systems remain large enough for the message-passing to be valid inside each of them: each sub-system must itself be a mean-field system, which is true if $L \gg L_c$. Concurrently, however, the larger L_c , the better it is to get closer to the optimal threshold. This is due to the fact that the overall rate is a weighted average of the effective rate of the seed block R_{seed} and that of the remaining ones R_{rest} . From (45) combined with (1) we deduce:

$$R = \frac{L_c R_{rest} R_{seed}}{(L_r - 1) R_{seed} + R_{rest}} \xrightarrow{L_c, L_r \gg 1} R_{rest} \quad (98)$$

where R_{rest} can be asymptotically as large as the Bayes optimal rate $R_{opt}(B)$ defined as the highest rate until which the superposition codes scheme allows to decode the input message for a given section size B . This threshold will be defined more precisely in Sec. VI.

A. Derivation of the state evolution in the spatially coupled operator case

The derivation of the state evolution in the spatially coupled case is very similar to the full operator case, see previous Sec. IV, with the difference that now each block can have different variances, and thus one must be vigilant when performing the derivation. We give here the main steps, the details being similar to the previous section. All the computations are done keeping in mind the limit $L \gg L_c, L_r$ in which AMP is valid with spatial coupling. As before, starting from the algorithm Fig. 4 and the operators definitions (43), (44):

$$\mathbf{R}_l^{t+1} = \mathbf{a}_l^t + (\Sigma_l^{t+1})^2 \sum_r \sum_{\mu \in \mathbf{r}} \frac{\alpha_r N / L_c}{1/\text{snr} + \Theta_\mu^{t+1}} \left[\sum_c \sum_{k \in \mathbf{c}} \mathbf{F}_{\mu k}^T (\mathbf{x}_k - \mathbf{a}_k^t) + \xi_\mu + \underbrace{\Theta_\mu^{t+1} \frac{y_\mu - w_\mu^t}{1/\text{snr} + \Theta_\mu^t}}_{:= \Lambda_\mu^t} \right] \quad (99)$$

Now we notice from the fact that the variances depends only on the block indices that:

$$\Theta_\mu = \sum_c \sum_{l \in \mathbf{c}} (\mathbf{F}_{\mu l}^2)^T \mathbf{v}_l \approx \sum_c \frac{J_{r_{\mu, \mathbf{c}}}}{L} \sum_{l \in \mathbf{c}} \sum_{i \in \mathbf{l}} v_i =: \Theta_{r_\mu} \quad (100)$$

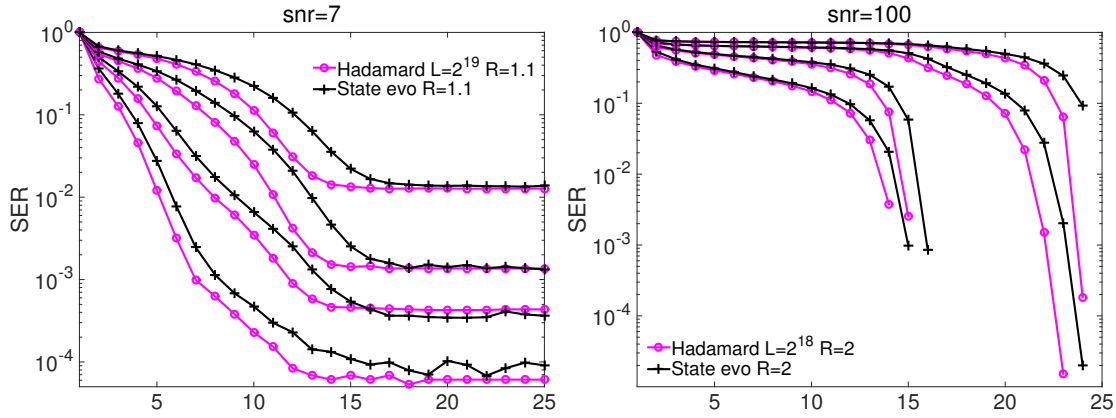


Fig. 9. The state evolution prediction of the section error rate $\{\text{SER}_c^t : c \in \{1, \dots, L_c = 4\}\}$ for each of the four induced block of the signal (see Fig. 5) as a function of time (black curves), compared to the actual $\{\text{SER}_c^t\}$ of the algorithm for $\text{snr} = 7/100$, different rates R , a section size $B = 32$, different signal size L values in the spatially coupled Hadamard operator case. The operator is drawn from the ensemble ($L_c = 4, L_r = 5, w = 2, \sqrt{J} = 0.6, R, \beta_{\text{seed}} = 1.5$). The power allocation is constant. The state evolution is computed by monte carlo technique with a sample size of 10^6 . The finite size curves at high snr stop without reaching a threshold because the recovery is actually perfect and the final $\text{SER} = 0$ which is due to the finite size effects, the same happens for the theoretical curves that reach 0 due to finite numerical precision. In the low $\text{snr} = 7$ case, the error floor (different in each block) is well predicted by state evolution.

where $J_{r,c}$ is the not yet rescaled by $1/L$ variance of the elements of the block of the spatially coupled operator that is at the r^{th} line of blocks, c^{th} column of blocks, see Fig. 5 and the notation $r_\mu(c_l)$ means the block index $r \in \{1, \dots, L_r\}$ ($c \in \{1, \dots, L_c\}$) to which the factor index μ (variable index l) belongs to. It follows from the definition of $(\Sigma_l^{t+1})^2$ in Fig. 4 that:

$$(\Sigma_l^{t+1})^2 = \frac{L_c}{B} \left(\sum_r \frac{J_{r,c_l} \alpha_r}{1/\text{snr} + \Theta_r^{t+1}} \right)^{-1} \mathbf{1}_B \quad (101)$$

α_r, L_c and L_r are defined in the subsection of Sec. III about the fast Hadamard operator construction. We deduce the expression of \mathbf{R}_l^{t+1} :

$$\begin{aligned} \mathbf{R}_l^{t+1} &\approx \mathbf{a}_l + (\Sigma_l^{t+1})^2 \sum_r \frac{1}{1/\text{snr} + \Theta_r^{t+1}} \sum_{\mu \in \mathbf{r}}^{\alpha_r N/L_c} \mathbf{F}_{\mu l} \left[\sum_c \sum_{k \in \mathbf{c}: k \neq l}^{L/L_c} \mathbf{F}_{\mu k}^T (\mathbf{x}_k - \mathbf{a}_k^t) + \xi_\mu + \Lambda_\mu^t \right] \\ &\quad + \underbrace{(\Sigma_l^{t+1})^2 \sum_r \frac{1}{1/\text{snr} + \Theta_r^{t+1}} \sum_{\mu \in \mathbf{r}}^{\alpha_r N/L_c} \mathbf{F}_{\mu l} \left[\mathbf{F}_{\mu l}^T (\mathbf{x}_l - \mathbf{a}_l) \right]}_{:=U} \end{aligned} \quad (102)$$

$$\approx \mathbf{x}_l + \underbrace{(\Sigma_l^{t+1})^2 \sum_r \frac{1}{1/\text{snr} + \Theta_r^{t+1}} \sum_{\mu \in \mathbf{r}}^{\alpha_r N/L_c} \mathbf{F}_{\mu l} \left[\sum_c \sum_{k \in \mathbf{c}: k \neq l}^{L/L_c} \mathbf{F}_{\mu k}^T (\mathbf{x}_k - \mathbf{a}_k^t) + \xi_\mu + \Lambda_\mu^t \right]}_{:=\mathbf{r}_{rl}^{t+1}} \quad (103)$$

where we have used the same approximation as in (70) and:

$$U = (\Sigma_l^{t+1})^{-2} (\mathbf{x}_l - \mathbf{a}_l) + O(1/\sqrt{L}) \quad (104)$$

$$\Lambda_\mu^t := \Theta_{r_\mu}^{t+1} \frac{y_\mu - w_\mu^t}{1/\text{snr} + \Theta_{r_\mu}^t} \quad (105)$$

In addition we define:

$$\mathbf{r}_l^{t+1} := (\Sigma_l^{t+1})^2 \sum_r \frac{\mathbf{r}_{rl}^{t+1}}{1/\text{snr} + \Theta_r^{t+1}} \quad (106)$$

We can now compute by central limit theorem the moments of the Gaussian distributed variables \mathbf{r}_{rl}^{t+1} in order to deduce the moments of \mathbf{r}_l^{t+1} . As in the previous section, we only keep the $O(1)$ terms. We can actually identify \mathbf{r}_{rl}^{t+1} to \mathbf{r}^{t+1} of (68) and thus, the computations are exactly the same as for the full operator case up to the values of the variances that are different. Using again (37), (71) remains valid, so that we get a similar result to (73) and (74):

$$\mathbb{E}_{\mathbf{F}, \xi, \mathbf{x}} \{\mathbf{r}_{rl}^{t+1}\} \approx \mathbf{0}_B \rightarrow \mathbb{E}_{\mathbf{F}, \xi, \mathbf{x}} \{\mathbf{r}_l^{t+1}\} \approx \mathbf{0}_B \quad (107)$$

The cross terms cancel as well by independence of the matrix elements, and thus of the \mathbf{r}_{rl}^{t+1} variables:

$$\mathbb{E}_{\mathbf{F}, \xi, \mathbf{x}} \{ \mathbf{r}_l^{t+1} \mathbf{r}_{l'}^{t+1} \}_{l' \neq l} = (\Sigma_l^{t+1})^2 (\Sigma_{l'}^{t+1})^2 \sum_{r, r'}^{L_r, L_r} \frac{\mathbb{E}_{\mathbf{F}, \xi, \mathbf{x}} \{ \mathbf{r}_{rl}^{t+1} \} \mathbb{E}_{\mathbf{F}, \xi, \mathbf{x}} \{ \mathbf{r}_{r'l'}^{t+1} \}}{(1/\text{snr} + \Theta_r^{t+1})(1/\text{snr} + \Theta_{r'}^{t+1})} \approx \mathbf{0}_B \quad (108)$$

The only moment that changes is the variance term. Skipping some steps similar to (78), (79), we get:

$$\begin{aligned} \mathbb{E}_{\mathbf{F}, \xi, \mathbf{x}} \{ (\mathbf{r}_{rl}^{t+1})^2 \} &= \mathbb{E}_{\mathbf{F}, \xi, \mathbf{x}} \left\{ \sum_{\mu \in \mathbf{r}}^{\alpha_r N / L_c} \mathbf{F}_{\mu l}^2 \left[\sum_c^{L_c} \sum_{k \in \mathbf{c}; k \neq l}^{L/L_c} \mathbf{F}_{\mu k}^T (\mathbf{x}_k - \mathbf{a}_k^t) \right] \left[\sum_{c'}^{L_c} \sum_{k' \in \mathbf{c}'; k' \neq l}^{L/L_c} \mathbf{F}_{\mu k'}^T (\mathbf{x}_{k'} - \mathbf{a}_{k'}^t) \right] \right\} \\ &+ \mathbb{E}_{\mathbf{F}, \xi, \mathbf{x}} \left\{ \sum_{\mu \in \mathbf{r}}^{\alpha_r N / L_c} \mathbf{F}_{\mu l}^2 \zeta_\mu^2 \right\} + \underbrace{\mathbb{E}_{\mathbf{F}, \xi, \mathbf{x}} \left\{ \sum_{\mu \in \mathbf{r}}^{\alpha_r N / L_c} \mathbf{F}_{\mu l}^2 \Lambda_\mu^2 \right\}}_{\in O(L^{-3/2})} + 2 \underbrace{\mathbb{E}_{\mathbf{F}, \xi, \mathbf{x}} \left\{ \sum_{\mu \in \mathbf{r}}^{\alpha_r N / L_c} \mathbf{F}_{\mu l}^2 \Lambda_\mu \left[\sum_c^{L_c} \sum_{k \in \mathbf{c}; k \neq l}^{L/L_c} \mathbf{F}_{\mu k}^T (\mathbf{x}_k - \mathbf{a}_k^t) \right] \right\}}_{= \mathbf{0}_B} \end{aligned} \quad (109)$$

$$\approx \mathbb{E}_{\mathbf{F}, \xi, \mathbf{x}} \left\{ \sum_{\mu \in \mathbf{r}}^{\alpha_r N / L_c} \mathbf{F}_{\mu l}^2 \left[\sum_c^{L_c} \sum_{k \in \mathbf{c}; k \neq l}^{L/L_c} (\mathbf{F}_{\mu k}^2)^T (\mathbf{x}_k - \mathbf{a}_k^t)^2 \right] \right\} + \frac{\alpha_r B J_{r, c_l}}{\text{snr} L_c} \quad (110)$$

$$\approx \frac{\alpha_r B J_{r, c_l}}{\text{snr} L_c} + \sum_{\mu \in \mathbf{r}}^{\alpha_r N / L_c} \frac{J_{r, c_l}}{L} \left[\sum_c^{L_c} \frac{J_{r, c_c}}{L} \sum_{k \in \mathbf{c}; k \neq l}^{L/L_c} \underbrace{\mathbb{E}_{\mathbf{F}, \xi, \mathbf{x}} \{ (\mathbf{x}_k - \mathbf{a}_k^t)^T (\mathbf{x}_k - \mathbf{a}_k^t) \}}_{\approx \tilde{E}_c N / L_c} \right] \quad (111)$$

$$= \frac{\alpha_r B J_{r, c_l}}{L_c} \left(\frac{1}{\text{snr}} + \frac{B}{L_c} \sum_c^{L_c} J_{r, c_c} \tilde{E}_c \right) \quad (112)$$

$$\tilde{E}_c := \frac{L_c}{N} \sum_{k \in \mathbf{c}}^{L/L_c} \mathbb{E}_{\mathbf{F}, \xi, \mathbf{x}} \{ (\mathbf{x}_k - \mathbf{a}_k^t)^T (\mathbf{x}_k - \mathbf{a}_k^t) \} \quad (113)$$

where \tilde{E}_c is the biased MSE of the block c of the signal, where the block structure of the signal is induced by the design of the spatially coupled operator, see Fig. 5. The variance of \mathbf{r}_r^{t+1} is deduced from (107) using again the independence of the matrix elements:

$$\mathbb{E}_{\mathbf{F}, \xi, \mathbf{x}} \{ (\mathbf{r}_l^{t+1})^2 \} = (\Sigma_l^{t+1})^4 \sum_{r, r'}^{L_r, L_r} \frac{\mathbb{E}_{\mathbf{F}, \xi, \mathbf{x}} \{ \mathbf{r}_{rl}^{t+1} \mathbf{r}_{r'l}^{t+1} \}}{(1/\text{snr} + \Theta_r^{t+1})(1/\text{snr} + \Theta_{r'}^{t+1})} = (\Sigma_l^{t+1})^4 \sum_r^{L_r} \frac{\mathbb{E}_{\mathbf{F}, \xi, \mathbf{x}} \{ (\mathbf{r}_{rl}^{t+1})^2 \}}{(1/\text{snr} + \Theta_r^{t+1})^2} \quad (114)$$

We define the average variance of the estimates inside the block c as:

$$\tilde{V}_c := L_c / N \sum_{l \in \mathbf{c}}^{L/L_c} \sum_{i \in \mathbf{l}}^B v_i \quad (115)$$

The matching prior condition, referred to as the Nishimori condition in statistical physics, allows to greatly simplify the results. It implies an equality between the mean variance per block and the biased MSE per block. The demonstration of this condition can be found in [12]. It becomes $\tilde{V}_c = \tilde{E}_c \forall c \in \{1, \dots, L_c\}$. From this and (100), we can rewrite Θ_r as:

$$\Theta_r = B / L_c \sum_c^{L_c} J_{r, c} \tilde{V}_c = B / L_c \sum_c^{L_c} J_{r, c} \tilde{E}_c \quad (116)$$

We plug this expression into (112) and using (114), (101) we get:

$$\mathbb{E}_{\mathbf{F}, \xi, \mathbf{x}} \{ (\mathbf{r}_l^{t+1})^2 \} = (\Sigma_l^{t+1})^4 B / L_c \sum_r^{L_r} \frac{\alpha_r J_{r, c_l} (1/\text{snr} + \Theta_r^{t+1})}{(1/\text{snr} + \Theta_r^{t+1})^2} = (\Sigma_l^{t+1})^2 \quad (117)$$

So now we know the distribution of R_i^{t+1} from (103):

$$r_i^{t+1} \sim \mathcal{N}_{0, (\tilde{\Sigma}_i^{t+1})^2} \rightarrow R_i^{t+1} \sim \mathcal{N}_{x_i, (\tilde{\Sigma}_i^{t+1})^2} \quad (118)$$

$$\tilde{\Sigma}_c^{t+1} (\{E_{c'}^t : c' \in \{1, \dots, L_c\}\}) = \left[B \sum_r^{L_r} \frac{\alpha_r J_{rc}}{L_c / \text{snr} + B \sum_{c'}^{L_c} J_{rc'} \tilde{E}_{c'}} \right]^{-1/2} \quad (119)$$

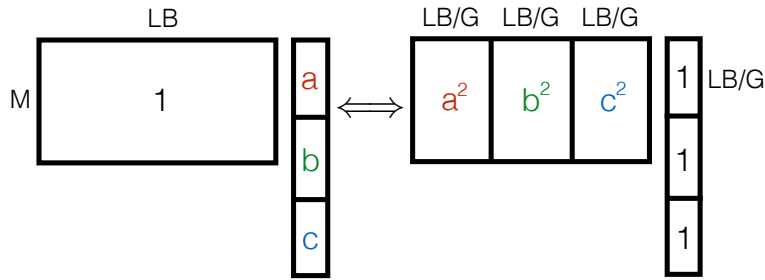


Fig. 10. The figure shows how to convert a non constant power allocated signal encoded through a full operator with elements of variance 1 into an equivalent system with constant power allocation encoded by a structured operator. The values on the matrix represent the variance of the elements of the matrix (we drop here the rescaling by $1/L$), the values on the matrix represent the non zero values of the sections that belong to a given group: here the signal is decomposed into $G = 3$ groups, and all the sections inside the first group have a non zero value equal to a , and so on. The transformation is done by structuring the operator into block columns, with as many block columns as different values in the power allocation, or groups: if a column of the original matrix acts on a component of a section where the non zero value is u , then this column variance is multiplied by u^2 in the new structured operator (such that the elements of this column are multiplied by u). The different sizes of the matrix or groups are represented.

Defining the rescaled biased MSE by block $E_c^t := B\tilde{E}_c^t$ and rescaled $\Sigma_c^{t+1} := \tilde{\Sigma}_c^{t+1}\sqrt{\log(B)}$, from the same arguments as in the previous section, we finally obtain the following state evolution over the biased MSE E_c inside the block c in the $L \rightarrow \infty$ limit:

$$E_c^{t+1} = \int \mathcal{D}\mathbf{z} ([f_{a_{11}}((\Sigma_c^{t+1})^2, \mathbf{z}) - 1]^2 + (B-1)f_{a_{21}}((\Sigma_c^{t+1})^2, \mathbf{z})^2) \quad (120)$$

$$\Sigma_c^{t+1}(\{E_{c'}^t : c' \in \{1, \dots, L_c\}\}) = \sqrt{\log(B)/B} \left[\sum_r \frac{\alpha_r J_{rc}}{L_c/\text{snr} + \sum_{c'} J_{rc'} E_{c'}^t} \right]^{-1/2} \quad (121)$$

where the f_a functions (92), (93) are defined in the previous section and where the mapping to the SER per block is given by:

$$\text{SER}_c^{t+1} = \int \mathcal{D}\mathbf{z} \mathbb{I}(\exists j \in \{2, \dots, B\} : f_{a_{j1}}((\Sigma_c^{t+1})^2, \mathbf{z}) > f_{a_{11}}((\Sigma_c^{t+1})^2, \mathbf{z})) \quad \forall c \in \{1, \dots, L_c\} \quad (122)$$

Thanks to this analysis, we can now predict the asymptotic SER per block in the signal estimate by the AMP decoder. Fig. 9 shows a comparison of the SER per block $\{\text{SER}_c^t : c \in \{1, \dots, L_c\}\}$ predicted by state evolution (black curves) with the actual SER per block of the superposition codes with AMP decoder combined with Hadamard based spatially coupled operators. The discrepancies between the theoretical and experimental curves come from the fact that state evolution is derived for random i.i.d Gaussian matrices, but the final error using these Hadamard operators is the same as predicted by state evolution as observed in the $\text{snr} = 7$ case. In the high snr regime, the curves stop for the same reasons as the Fig. 8 of the previous section and meaning that the decoding was perfect. As noted in [19], structured operators converge faster to the predicted final error than purely i.i.d matrices as predicted by the state evolution.

B. State evolution with power allocation

We now observe that we can trivially obtain the state evolution for a non constant power allocation of the signal encoded with a random full i.i.d Gaussian matrix from the previous analysis, thanks to the transformation of Fig. 10: starting from an homogeneous matrix and non constant power allocated signal, we convert the system into a structured matrix with a constant power allocated signal.

Suppose the signal is decomposed into G groups, where inside the group g , the power allocation is the same for all the sections belonging to this group and equals c_g . Now one must create a structured operator starting from the original one, decomposing it into LB/G column blocks and multiply all the elements of the column block g by c_g , as shown in Fig. 10. This new operator acting on a constant power allocated signal is totally equivalent to the original system and we have the state evolution of this new system from the previous analysis. Using (121) in the present setting, one has to be careful with the value of α_r defined as the number of lines over the number of columns of the block line r . Here there is a unique value that equals $M/(N/G) = G\alpha$ where α is defined as the original measurement rate (1). Given that, $L_c = G$ we finally obtain:

$$E_g^{t+1} = \int \mathcal{D}\mathbf{z} ([f_{a_{11}}((\Sigma_g^{t+1})^2, \mathbf{z}) - 1]^2 + (B-1)f_{a_{21}}((\Sigma_g^{t+1})^2, \mathbf{z})^2) \quad (123)$$

$$\Sigma_g^{t+1}(\{E_{g'}^t : g' \in \{1, \dots, G\}\}) = \sqrt{\log(B)/B} \left[\frac{\alpha c_g^2}{1/\text{snr} + 1/G \sum_{g'} c_{g'}^2 E_{g'}^t} \right]^{-1/2} \quad (124)$$

VI. REPLICA ANALYSIS

The replica analysis is a non-rigorous asymptotic $L \rightarrow \infty$ static statistical analysis (as opposed to the dynamical state evolution analysis) that allows the computation of the so-called replica free-entropy, a potential function of the SER. The method has been developed in the context of statistical physics of disordered systems [22] to compute thermodynamical averages over some source of disorder of any physical observable of the system, the reconstruction error in the present case. The method has then be extended to information theoretical problems [35, 36] due to the close connections between spin glass physics and communications problems such as the present one, where the sources of quenched disorder to average over are the noise, coding matrix and signal distributions.

A. Replica analysis with uniform power allocation

The following derivation follows closely the free-entropy calculation performed in [12] with the difference that in this context, computations are made considering each section as a B -d variable. We place ourselves in the constant power allocation case. We start from the definition of the potential at fixed section size B , or replica free-entropy that can be transformed using the replica trick:

$$\Phi_B := \lim_{L \rightarrow \infty} \frac{1}{L} \mathbb{E}_{\mathbf{F}, \boldsymbol{\xi}, \mathbf{x}} \{\log Z\} = \lim_{L \rightarrow \infty} \lim_{n \rightarrow 0} \frac{1}{L} \frac{\mathbb{E}_{\mathbf{F}, \boldsymbol{\xi}, \mathbf{x}} \{Z^n\} - 1}{n} \quad (125)$$

where $\mathbb{E}_{\mathbf{F}, \boldsymbol{\xi}, \mathbf{x}}$ is the average over all the sources of randomness and Z is the normalization constant of the full posterior distribution, also called the partition function, a random variable function of the disorder:

$$Z(\mathbf{F}, \boldsymbol{\xi}, \mathbf{x}) = \int \left[\prod_l^L d\hat{\mathbf{x}}_l P_0(\hat{\mathbf{x}}_l) \right] \prod_\mu^M \sqrt{\frac{\text{snr}}{2\pi}} e^{-\frac{\text{snr}}{2} (\sum_l^L \mathbf{F}_{\mu l}^T (\hat{\mathbf{x}}_l - \mathbf{x}_l) + \xi_\mu)^2} \quad (126)$$

Z^n is the so-called replicated partition function. As we have constant allocation, the prior is the same in every section such that we can drop the section index. The index associated to the replica is $a \in \{1, \dots, n\}$. From the definition of the prior (39), we get:

$$\mathbb{E}_{\mathbf{F}, \boldsymbol{\xi}, \mathbf{x}} \{Z^n\} = (\text{snr}/2\pi)^{\frac{Mn}{2}} \mathbb{E}_{\mathbf{x}} \left\{ \int \left[\prod_{l,a}^{L,n} d\hat{\mathbf{x}}_l^a P_0(\hat{\mathbf{x}}_l^a) \right] \prod_\mu^M X_\mu \right\} \quad (127)$$

$$X_\mu := \mathbb{E}_{\mathbf{F}, \boldsymbol{\xi}} \left\{ e^{-\frac{\text{snr}}{2} \sum_a^n (\sum_l^L \mathbf{F}_{\mu l}^T (\mathbf{x}_l - \hat{\mathbf{x}}_l^a) + \xi_\mu)^2} \right\} = \mathbb{E}_{\mathbf{F}, \boldsymbol{\xi}} \left\{ e^{-\frac{\text{snr}}{2} \sum_a^n (v_\mu^a)^2} \right\} \quad (128)$$

where we have defined $v_\mu^a := \sum_l^L \mathbf{F}_{\mu l}^T (\mathbf{x}_l - \hat{\mathbf{x}}_l^a) + \xi_\mu$. To compute X_μ (128), we can apply the central limit theorem to the quantity v_μ^a which is a sum of independent terms. We thus need its first two moments to define its associated Gaussian distribution:

$$\begin{aligned} \mathbb{E}_{\mathbf{F}, \boldsymbol{\xi}} \{v_\mu^a\} &= 0 \\ \mathbb{E}_{\mathbf{F}, \boldsymbol{\xi}} \{(v_\mu^a)^2\} &= \mathbb{E}_{\mathbf{F}, \boldsymbol{\xi}} \left\{ \sum_{l,k}^{L,L} [\mathbf{F}_{\mu l}^T (\mathbf{x}_l - \hat{\mathbf{x}}_l^a)]^T \mathbf{F}_{\mu k}^T (\mathbf{x}_k - \hat{\mathbf{x}}_k^a) + 2\xi_\mu \sum_l^L \mathbf{F}_{\mu l}^T (\mathbf{x}_l - \hat{\mathbf{x}}_l^a) + \xi_\mu^2 \right\} \\ &= \sum_{l,k}^{L,L} \left[(\mathbf{x}_l - \hat{\mathbf{x}}_l^a)^T \mathbb{E}_{\mathbf{F}} \left\{ \mathbf{F}_{\mu l} \mathbf{F}_{\mu k}^T \right\} (\mathbf{x}_k - \hat{\mathbf{x}}_k^a) \right] + 1/\text{snr} \end{aligned} \quad (130)$$

Using the fact that each element of the matrix is i.i.d, we find that only the diagonal elements of the matrix $\mathbb{E}_{\mathbf{F}} \left\{ \mathbf{F}_{\mu l} \mathbf{F}_{\mu k}^T \right\}$ are non zero:

$$\mathbb{E}_{\mathbf{F}} \left\{ \mathbf{F}_{\mu l} \mathbf{F}_{\mu k}^T \right\} = \frac{\delta_{k,l}}{L} \mathbf{I}_B \rightarrow \mathbb{E}_{\mathbf{F}, \boldsymbol{\xi}} \{(v_\mu^a)^2\} = 1/L \sum_l^L (\mathbf{x}_l - \hat{\mathbf{x}}_l^a)^T (\mathbf{x}_l - \hat{\mathbf{x}}_l^a) + 1/\text{snr} \quad (131)$$

where \mathbf{I}_B is the identity matrix of dimension $B \times B$. Now we define new macroscopic order parameters which will be considered as the new degrees of freedom of the replicated system, instead of the individual replica states $\{\hat{\mathbf{x}}_a\}$. In this way, we average out the microscopic properties of the system to get access to the macroscopic ones, the goal of the replica methodology:

$$m_a := 1/L \sum_l^L (\hat{\mathbf{x}}_l^a)^T \mathbf{x}_l, \quad Q_a := 1/L \sum_l^L (\hat{\mathbf{x}}_l^a)^T \hat{\mathbf{x}}_l^a, \quad q_{ab} := 1/L \sum_l^L (\hat{\mathbf{x}}_l^a)^T \hat{\mathbf{x}}_l^b \quad (132)$$

m_a is the overlap between the replica state $\hat{\mathbf{x}}^a$ and the signal \mathbf{x} , Q_a is the power of the replica a and q_{ab} is the overlap between replicas a and b . Rewriting the previous moment (131) in terms of these new quantities, we get:

$$\mathbb{E}_{\mathbf{F}, \boldsymbol{\xi}} \{ (v_\mu^a)^2 \} = 1/L \underbrace{\sum_l \mathbf{x}_l^T \mathbf{x}_l}_{:= \langle x^2 \rangle_L} - 2m_a + Q_a + 1/\text{snr} = 1 - 2m_a + Q_a + 1/\text{snr} \quad (133)$$

Exactly in the same way, we get the cross terms $\forall a \neq b$:

$$\mathbb{E}_{\mathbf{F}, \boldsymbol{\xi}} \{ v_\mu^a v_\mu^b \} = 1 - (m_a + m_b) + q_{ab} + 1/\text{snr} \quad (134)$$

We now assume the replica symmetric ansatz, which is valid for inference problems (and more generally planted problems) on locally tree-like or highly dense graphs such as in the present case, see [22] for more details:

$$q_{ab} = q \quad \forall (a, b : a \neq b), \quad Q_a = Q \quad \forall a, \quad m_a = m \quad \forall a \quad (135)$$

The covariance matrix \mathbf{G} of $\{v_\mu^a\}$ under this ansatz reads $\forall (a, b)$:

$$G_{ab} := \mathbb{E}_{\mathbf{F}, \boldsymbol{\xi}} \{ v_\mu^a v_\mu^b \} = 1 - 2m + 1/\text{snr} + q + (Q - q)\delta_{a,b} \quad (136)$$

$$\rightarrow \mathbf{G} = (1 - 2m + 1/\text{snr} + q) \mathbf{1}_n + (Q - q) \mathbf{I}_n \quad (137)$$

where $\mathbf{1}_n$ is a matrix full of ones of dimension $n \times n$. We thus have:

$$X_\mu = \mathbb{E}_{\mathbf{v}} \{ e^{-\frac{\text{snr}}{2} \mathbf{v}^T \mathbf{v}} \}, \quad P(\mathbf{v}) = [(2\pi)^n \det(\mathbf{G})]^{-1/2} e^{-\frac{1}{2} \mathbf{v}^T \mathbf{G}^{-1} \mathbf{v}} \quad (138)$$

The explicit computation of X_μ by Gaussian integral gives:

$$X_\mu = [(2\pi)^n \det(\mathbf{G})]^{-1/2} \int d\mathbf{v} e^{-\frac{1}{2} \mathbf{v}^T (\mathbf{G}^{-1} + \text{snr} \mathbf{I}_n) \mathbf{v}} = 1/\sqrt{\det(\mathbf{I}_n + \text{snr} \mathbf{G})} \quad (139)$$

The eigenvectors of \mathbf{G} are one eigenvector $(1, 1, \dots, 1)$ with associated eigenvalue $Q - q + n(1 - 2m + 1/\text{snr} + q)$ and $n - 1$ eigenvectors of the type $(0, \dots, 0, -1, 1, 0, \dots, 0)$ with degenerated eigenvalue $Q - q$. Therefore:

$$\det(\mathbf{I}_n + \text{snr} \mathbf{G}) = \frac{1 + \text{snr} [Q - q + n(1 - 2m + 1/\text{snr} + q)]}{[1 + \text{snr}(Q - q)]^{1-n}} \quad (140)$$

from which we get:

$$\lim_{n \rightarrow 0} X_\mu = e^{-\frac{n}{2} \left[\frac{q - 2m + 1 + 1/\text{snr}}{Q - q + 1/\text{snr}} + \log(1/\text{snr} + Q - q) - \log(1/\text{snr}) \right]} \quad (141)$$

We need to enforce the constraints that the new order parameters satisfy their definitions (132). This is done by the usual trick of rewriting 1 as the inverse Fourier transform of its Fourier transform and plugging this expression in the definition of the averaged replicated partition function that we are computing:

$$1 = \int \left[\prod_a^n dQ_a d\hat{Q}_a dm_a d\hat{m}_a \right] \left[\prod_{b,a < b}^{n(n-1)/2} dq_{ab} d\hat{q}_{ab} \right] \exp \left[-\sum_a^n \hat{m}_a (m_a L - \sum_l^L (\hat{\mathbf{x}}_l^a)^T \mathbf{x}_l) + \sum_a^n \hat{Q}_a (Q_a L/2 - 1/2 \sum_l^L (\hat{\mathbf{x}}_l^a)^T \hat{\mathbf{x}}_l^a) - \sum_{b,a < b}^{n(n-1)/2} \hat{q}_{ab} (q_{ab} L - \sum_l^L (\hat{\mathbf{x}}_l^a)^T \hat{\mathbf{x}}_l^b) \right] \quad (142)$$

$$\rightarrow \mathbb{E}_{\mathbf{F}, \boldsymbol{\xi}, \mathbf{x}} \{ Z^n \} = \int \left[\prod_a^n dQ_a d\hat{Q}_a dm_a d\hat{m}_a \right] \left[\prod_{b,a < b}^{n(n-1)/2} dq_{ab} d\hat{q}_{ab} \right] e^{L \left(\frac{1}{2} \sum_a^n \hat{Q}_a Q_a - \frac{1}{2} \sum_{b,a < b}^{n(n-1)/2} \hat{q}_{ab} q_{ab} - \sum_a^n \hat{m}_a m_a \right)} \left[\prod_\mu^M X_\mu \right] \underbrace{\left(\int d\mathbf{x} P_0(\mathbf{x}) \left[\prod_a^n P_0(\hat{\mathbf{x}}^a) \right] e^{-\frac{1}{2} \sum_a^n \hat{Q}_a (\hat{\mathbf{x}}^a)^T \hat{\mathbf{x}}^a + \frac{1}{2} \sum_{b,a < b}^{n(n-1)/2} \hat{q}_{ab} (\hat{\mathbf{x}}^a)^T \hat{\mathbf{x}}^b + \sum_a^n \hat{m}_a (\hat{\mathbf{x}}^a)^T \mathbf{x}} \right)}_{:= \Gamma} (\text{snr}/2\pi)^{\frac{Mn}{2}} \quad (143)$$

We define:

$$\tilde{\Gamma} := \int d\mathbf{x} \mathcal{D}\mathbf{z} P_0(\mathbf{x}) \underbrace{\left[\int d\hat{\mathbf{x}} P_0(\hat{\mathbf{x}}) e^{-\frac{1}{2} (\hat{Q} + \hat{q}) \hat{\mathbf{x}}^T \hat{\mathbf{x}} + \hat{m} \hat{\mathbf{x}}^T \mathbf{x} + \mathbf{z}^T \hat{\mathbf{x}} \sqrt{\hat{q}}} \right]^n}_{:= f(\mathbf{z})} \quad (144)$$

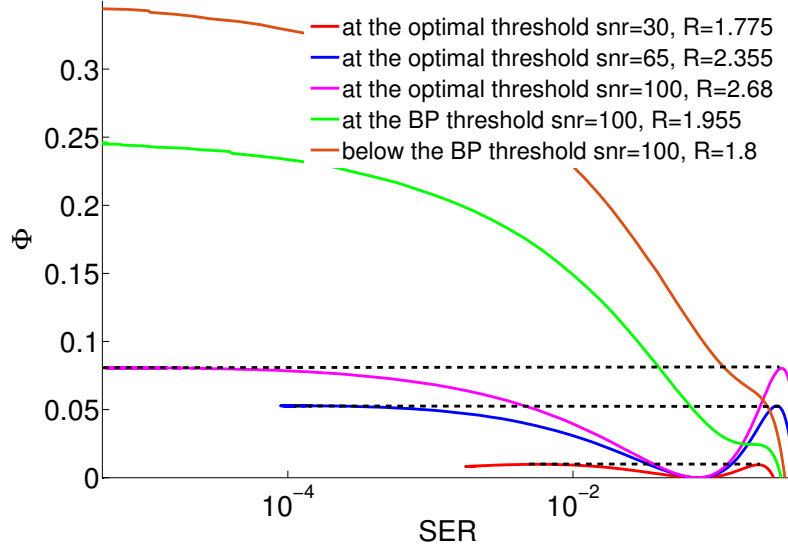


Fig. 11. The free-entropy (or potential) Φ as a function of the section-error rate SER for $B = 2$, different rates and snr. The maxima of the curves corresponds to the typical SER values which are fixed points of the state evolution equations (94) for a given set of parameters (R, B, snr) . The global maximum corresponds to the (exponentially) most probable SER solution (the equilibrium state), referred as the optimal SER*. The curves are obtained by numerical integration of (155). The optimal threshold R_{opt} is defined as the rate where the high and low error maxima have same height (i.e same probability), see pink, blue and red curves. The BP threshold R_{BP} corresponds to the rate at which the metastable state a high error that blocks the convergence of AMP appears, see green curve. The plot illustrates how the gap at the optimal threshold between the two maxima increases with the snr. This explains why it is easier to decode closer to the optimal threshold for larger snr. $\text{snr} = 100$: Here for rates larger than $R > 2.68$, the optimal SER* jumps from a low value to a large $O(1)$ one (pink curve). This defines the maximum possible rate (to compare here to $C = 3.3291$) below which acceptable performance can be obtained with AMP combined with spatial coupling or non constant power allocation. For $R < 2.68$, the SER* is much lower (and decay with R). The AMP decoder Fig. 4 allows to perform an ascent of this function. As long as the maximum is unique (i.e. for $R < 1.955$, see green curve), it will be able to achieve the predicted optimal performance with no need of spatial coupling or non constant power allocation in the large size limit, as in the case of the brown curve.

Using the stratanovitch transformation in B dimensions, given by:

$$e^{\frac{\hat{q}}{2} \sum_{b,a < b}^{n(n-1)/2} \hat{\mathbf{x}}_a^T \hat{\mathbf{x}}_b} = \prod_i^B e^{\frac{\hat{q}}{2} \sum_{b,a < b}^{n(n-1)/2} \hat{x}_{a,i} \hat{x}_{b,i}} = \prod_i^B \int \mathcal{D}z_i e^{\sqrt{\hat{q}} z_i \sum_a^n \hat{x}_{a,i} - \frac{\hat{q}}{2} \sum_a^n \hat{x}_{a,i}^2} = \int \mathcal{D}\mathbf{z} e^{\sqrt{\hat{q}} \mathbf{z}^T \sum_a^n \mathbf{x}_a} e^{-\frac{\hat{q}}{2} \sum_a^n \hat{\mathbf{x}}_a^T \hat{\mathbf{x}}_a} \quad (145)$$

we obtain under the replica symmetric ansatz that $\tilde{\Gamma} = \Gamma$. In addition we have:

$$\int \mathcal{D}\mathbf{z} f(\mathbf{z})^n \underset{n \rightarrow 0}{\approx} e^{n \int \mathcal{D}\mathbf{z} \log f(\mathbf{z})} \rightarrow \tilde{\Gamma} \underset{n \rightarrow 0}{\approx} e^{n \int d\mathbf{x} P_0(\mathbf{x}) \int \mathcal{D}\mathbf{z} \log f(\mathbf{z})} \quad (146)$$

Combining (146) and (143) under the replica symmetric ansatz, we get the expression of the averaged replicated partition function:

$$\mathbb{E}_{\mathbf{F}, \xi, \mathbf{x}} \{Z^n\} = \int dQ d\hat{Q} d\hat{m} d\hat{q} d\hat{q} e^{nL \tilde{\Phi}_B(m, \hat{m}, \hat{q}, \hat{q}, Q, \hat{Q})} \quad (147)$$

$$\begin{aligned} \tilde{\Phi}_B(m, \hat{m}, \hat{q}, \hat{q}, Q, \hat{Q}) &= \frac{1}{2} \left(\hat{Q}Q + \hat{q}\hat{q} - 2\hat{m}m \right) - \frac{\alpha B}{2} \left(\frac{q - 2m + \langle x^2 \rangle_L + 1/\text{snr}}{Q - q + 1/\text{snr}} + \log(1/\text{snr} + Q - q) \right) \\ &+ \int d\mathbf{x} P_0(\mathbf{x}) \mathcal{D}\mathbf{z} \log \left(\int d\hat{\mathbf{x}} P_0(\hat{\mathbf{x}}) e^{\hat{m}\mathbf{x}^T \hat{\mathbf{x}} + \sqrt{\hat{q}} \mathbf{z}^T \mathbf{x} - \frac{1}{2}(\hat{q} + \hat{Q}) \hat{\mathbf{x}}^T \hat{\mathbf{x}}} \right) \end{aligned} \quad (148)$$

For the replica trick (125) to be formally valid, the limit $n \rightarrow 0$ should taken before the limit over L . But we need to estimate the integral (147) by its saddle point, which is justified only if the limit $L \rightarrow \infty$ is performed before the limit over n . We thus assume that the limits commute, which is not rigorous, but heuristically verified in many different models, including inference problems. The saddle point estimate is performed by taking the optimum of $\tilde{\Phi}_B$, given by its fixed point value with respect to its different free parameters, which actually corresponds to the desired replica free-entropy as seen from (125):

$$\Phi_B := \tilde{\Phi}_B(m^*, \hat{m}^*, q^*, \hat{q}^*, Q^*, \hat{Q}^*) \quad (149)$$

The optimization gives these fixed point values, denoted with stars:

$$\frac{\partial \tilde{\Phi}_B}{\partial m} = 0 \rightarrow \hat{m}^* = \frac{\alpha B}{Q^* - q^* + 1/\text{snr}} \quad (150)$$

$$\frac{\partial \tilde{\Phi}_B}{\partial q} = 0 \rightarrow \hat{q}^* = \alpha B \frac{1/\text{snr} + \langle x^2 \rangle_L - 2m^* + q^*}{(Q^* - q^* + 1/\text{snr})^2} \quad (151)$$

$$\frac{\partial \tilde{\Phi}_B}{\partial Q} = 0 \rightarrow \hat{Q}^* = \alpha B \frac{2m^* - \langle x^2 \rangle_L - 2q^* + Q^*}{(Q^* - q^* + 1/\text{snr})^2} \quad (152)$$

In addition the matching prior condition implies:

$$q^* = m^*, \quad Q^* = \langle x^2 \rangle_L = 1, \quad E = \langle x^2 \rangle_L - m^* \quad (153)$$

$$\rightarrow \hat{q}^* = \hat{m}^* = \frac{\alpha B}{E + 1/\text{snr}} = \frac{\log(B)}{\Sigma(E)^2}, \quad \hat{Q}^* = 0 \quad (154)$$

where E is the rescaled biased MSE defined together with $\Sigma(E)$ by (90) and we have used (1) to get rid of α . Rewriting everything in terms of only $O(1)$, we get the final expression of the potential function for sparse superposition codes at fixed section size B :

$$\Phi_B(E) = -\frac{\log(B)}{2R \log(2)} \left(\log(1/\text{snr} + E) + \frac{1-E}{1/\text{snr} + E} \right) + \int \mathcal{D}\mathbf{z} \log \left(e^{\frac{\log(B)}{2\Sigma(E)^2} + \frac{\sqrt{\log(B)}z_1}{\Sigma(E)}} + \sum_{i=2}^B e^{-\frac{\log(B)}{2\Sigma(E)^2} + \frac{\sqrt{\log(B)}z_i}{\Sigma(E)}} \right) \quad (155)$$

Going from this expression to $\Phi_B(\text{SER})$ is possible thanks to (94).

The MSE values associated to the maxima of this potential correspond to fixed points of the state evolution equations (91) (again, speaking of MSE or SER is the same thanks to (94)). The information brought by this analysis, not explicitly included in the state evolution analysis, is the identification of the phase in which the system is (easy/hard/impossible inference) for a given set of parameters (R, B, snr) .

An example of such a potential (155) in the $(R, B = 2, \text{snr} = 100)$ case is shown on Fig. 11. The AMP algorithm follows a dynamics that can be interpreted as a gradient ascent in this free-entropy space, which starts the ascent from an high error state (a random guess for the signal estimate). The brown curve thus corresponds to an easy case as the global maximum is unique and corresponds to a low error state. The green curve corresponds to a the BP threshold, which marks the appearance of the hard inference phase. A second maxima appears at high error, blocking the convergence to the low error state. Still, the low error state has a higher free-entropy meaning it has an exponentially more important statistical weight and thus corresponds to the true equilibrium state. The problem is to reach it despite of the high error metastable state. Spatial coupling has been specifically designed to achieve this goal. The pink curve marks the appearance of the impossible inference phase defined as the rate where the low and high error states have same free-entropy. At any rate above, the low error state becomes metastable (then even disappears) and is no longer the equilibrium. Until this rate, the AMP algorithm combined with spatial coupling or well designed power allocation is theoretically able to decode, see Sec. VII and Sec. VIII.

B. The link between replica and state evolution analysis

We now show that the fixed point conditions of the replica potential are giving back the state evolution recursion of the biased MSE, and thus of the section rate as well. To do so we will use the matching prior assumption or Nishimori condition in statistical physics terms. We refer the reader to [12] where the condition is fully derived for generic inference problems.

We restrict ourselves to the constant power allocation case but the derivation for generic power allocation is done in a similar manner. We start from the replica potential expression (148). The fixed point condition for m^* at the fixed point with respect to the conjugate parameters gives:

$$\frac{\partial \tilde{\Phi}_B(\hat{m}^*, \hat{q}^*, \hat{Q}^*)}{\partial \hat{m}} = 0 \rightarrow m^*(E) = \int d\mathbf{x} \mathcal{D}\mathbf{z} P_0(\mathbf{x}) \int d\hat{\mathbf{x}} P_0(\hat{\mathbf{x}}) \frac{1}{Z(\mathbf{x}, \mathbf{z}, E)} e^{\frac{\log(B)}{2\Sigma(E)^2} (2\mathbf{x}^T [\hat{\mathbf{x}} + \mathbf{z}\Sigma(E)/\sqrt{\log(B)}] - 1)} \mathbf{x}^T \hat{\mathbf{x}} \quad (156)$$

where $Z(\mathbf{x}, \mathbf{z}, E)$ is the partition function:

$$Z(\mathbf{x}, \mathbf{z}, E) := \int d\hat{\mathbf{x}} P_0(\hat{\mathbf{x}}) e^{\frac{\log(B)}{2\Sigma(E)^2} (2\mathbf{x}^T [\hat{\mathbf{x}} + \mathbf{z}\Sigma(E)/\sqrt{\log(B)}] - 1)} \quad (157)$$

After simplification, we obtain:

$$m^* = \int \mathcal{D}\mathbf{z} \frac{1}{Z_1(\mathbf{z}, E)} e^{\frac{\log(B)}{2\Sigma(E)^2} (2[1+z_1 \frac{\sqrt{\log(B)}}{\Sigma(E)}] - 1)} \quad (158)$$

$$Z_1(\mathbf{z}, E) := \sum_i^B e^{\frac{\log(B)}{2\Sigma(E)^2} (2[\delta_{i,1} + z_i \frac{\sqrt{\log(B)}}{\Sigma(E)}] - 1)} \quad (159)$$

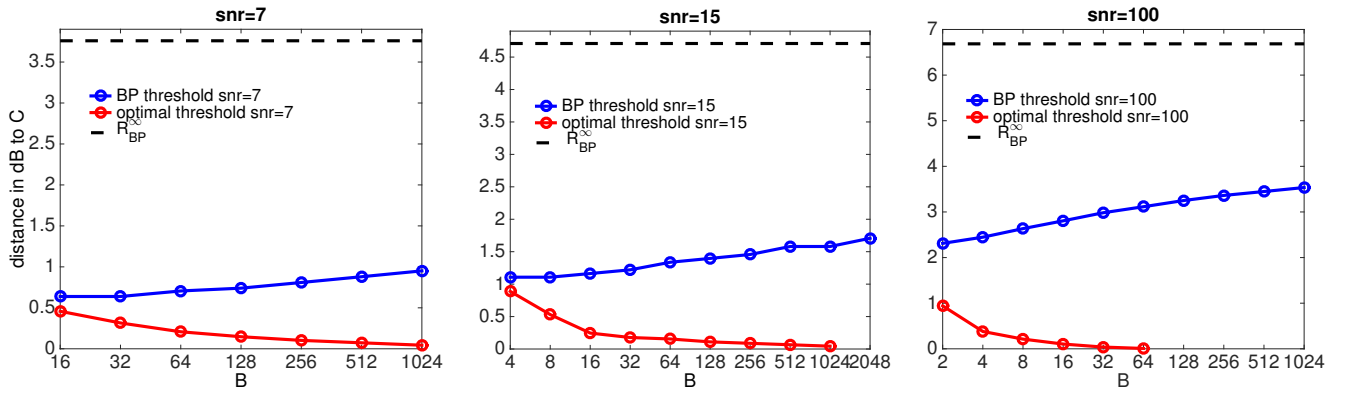


Fig. 12. All the points are computed by replica method from the potential (155) where the integral is computed by monte carlo method. These are the phase diagrams of the superposition codes for different snr, where the x axis is the section size B , the y axis is the distance to the capacity C in dB. The blue and red curves are respectively the BP and optimal threshold. The black dashed line is the asymptotic value of the BP threshold R_{BP}^∞ (171).

We thus recognize the expression (41) and using the definitions (88), (90) and (89) we obtain:

$$m^* = \int \mathcal{D}\mathbf{z} f_{a_1} \left((\tilde{\Sigma}^{t+1})^2, \mathbf{R}^{(1),t+1}(\mathbf{z}) \right) = \int \mathcal{D}\mathbf{z} f_{a_{11}} \left((\Sigma^{t+1})^2, \mathbf{z} \right) \quad (160)$$

Now using (153), we see that the fixed point of the replica potential gives back the state evolution (97). From this analysis, we can now assert that using the state evolution analysis to find fixed points of the decoder or extracting this information from the replica potential are totally equivalent. In addition, this validates further the replica analysis as an exact procedure in the present context.

C. Large section limit of the superposition codes

In order to get the asymptotic behavior in the section size of this potential, we need to compute the asymptotic value $I := \lim_{B \rightarrow \infty} I_B$ of the integral I_B that appears in (155). We shall drop the dependency of Σ in E to avoid confusions and compute:

$$I_B := \int \mathcal{D}\mathbf{z} \log \left(e^{\frac{\log(B)}{2\Sigma^2} + \frac{\sqrt{\log(B)}z_1}{\Sigma}} + \sum_{i=2}^B e^{-\frac{\log(B)}{2\Sigma^2} + \frac{\sqrt{\log(B)}z_i}{\Sigma}} \right) = \mathbb{E}_{\mathbf{z}} \{ \log(K_B) \} \quad (161)$$

We shall adopt here the vocabulary of statistical mechanics [22]: this is formally a problem of computing the average of the logarithm of a partition function of a system with B (disordered) states. Indeed, one can rewrite (161) as:

$$I_B = -\frac{\log(B)}{2\Sigma^2} + \int \mathcal{D}\mathbf{z} \log \left(e^{\frac{\log(B)}{\Sigma^2} + \frac{\sqrt{\log(B)}z_1}{\Sigma}} + \sum_{i=2}^B e^{\frac{\sqrt{\log(B)}z_i}{\Sigma}} \right) \quad (162)$$

$$= -\frac{\log(B)}{2\Sigma^2} + \int \mathcal{D}\mathbf{z} \log \left(\mathcal{Z}_1(z_1) + \mathcal{Z}_2(\{z_i : i \in \{2, \dots, B\}\}) \right) \quad (163)$$

where

$$\mathcal{Z}_1(z_1) := \exp \left(\log(B)/\Sigma^2 + \sqrt{\log(B)}z_1/\Sigma \right) \quad (164)$$

$$\mathcal{Z}_2(\{z_i : i \in \{2, \dots, B\}\}) := \sum_{i=2}^B \exp \left(\sqrt{\log(B)}z_i/\Sigma \right) \quad (165)$$

In fact \mathcal{Z}_2 is formally known as a random energy model in the statistical physics literature [22, 37], a statistical physics model where i.i.d energy levels are drawn from some given distribution. This analogy can be further refined by writing the energy as $U_i = -\sqrt{\log(B)}z_i$ and by denoting Σ as the temperature. In this case, a standard result [22, 37, 38] is:

- The asymptotic limit for large B of $\mathcal{J} := \log(\mathcal{Z}_2)/\log(B)$ exist, and is concentrated (i.e. it does not depend on the disorder realization).
- It is equal to $\mathcal{J} = \sqrt{2}/\Sigma \mathbb{I}(\Sigma < 1/\sqrt{2}) + (1/(2\Sigma^2) + 1) \mathbb{I}(\Sigma > 1/\sqrt{2})$

We can thus now obtain the value of the integral by comparing \mathcal{Z}_1 and \mathcal{Z}_2 and keeping only the dominant term. First let us consider the case where $\Sigma < 1/\sqrt{2}$:

$$\frac{1}{\log(B)} \log(\mathcal{Z}_1 + \mathcal{Z}_2) = \frac{1}{\log(B)} \left(\log(\mathcal{Z}_2) + \log\left(1 + \frac{\mathcal{Z}_1}{\mathcal{Z}_2}\right) \right) \approx \frac{\log(\mathcal{Z}_2)}{\log(B)}. \quad (166)$$

If, however, $\Sigma > 1/\sqrt{2}$, then:

$$\frac{1}{\log(B)} \log(\mathcal{Z}_1 + \mathcal{Z}_2) = \frac{1}{\log(B)} \left(\log(\mathcal{Z}_1) + \log\left(1 + \frac{\mathcal{Z}_2}{\mathcal{Z}_1}\right) \right) \approx \frac{\log(\mathcal{Z}_1)}{\log(B)}. \quad (167)$$

This leads to:

$$\lim_{B \rightarrow \infty} \frac{I_B}{\log(B)} = \frac{1}{2\Sigma^2} \mathbb{I}(\Sigma < 1/\sqrt{2}) + \mathbb{I}(\Sigma > 1/\sqrt{2}) \quad (168)$$

From these results combined with (155), (90), we now can give the asymptotic value of the potential:

$$\phi(E) := \lim_{B \rightarrow \infty} \frac{\Phi_B(E)}{\log(B)} = -\frac{1}{2R \log(2)} \left(\log(1/\text{snr} + E) + \frac{1-E}{1/\text{snr} + E} \right) + \max\left(1, \frac{1}{2\Sigma^2(E)}\right) \quad (169)$$

with $\Sigma^2(E) = R \log(2)(1/\text{snr} + E)$, see (90).

Let us now look at the extrema of this potential. We see that we have to distinguish between the high error case ($\Sigma > 1/\sqrt{2}$ so that $E > 1/(2R \log(2)) - 1/\text{snr}$) and the low error one ($\Sigma < 1/\sqrt{2}$, so that $E < 1/(2R \log(2)) - 1/\text{snr}$).

In the high error case, the derivative of the potential is zero when:

$$\frac{1}{2R \log(2)} \left(\frac{1}{1/\text{snr} + E} - \frac{1/\text{snr} + 1}{(1/\text{snr} + E)^2} \right) = 0 \quad (170)$$

which happens when $E = 1$. Therefore, if both the condition $E = 1$ and $E > 1/(2R \log(2)) - 1/\text{snr}$ are met, there is a stable extremum to the replica potential at $E = 1$. The existence of this high-error extremum thus requires $1/(2R \log(2)) - 1/\text{snr} < 1$, and we thus define the critical rate beyond which the state at $E = 1$ is stable:

$$R_{BP}^\infty := [(1/\text{snr} + 1)2 \log(2)]^{-1} \quad (171)$$

Since we initialize the recursion at $E = 1$ when we attempt to reconstruct the signal with AMP, we see that R_{BP} is a crucial limit for the reconstruction ability by message passing.

In the low error case, the derivative of the potential is zero when:

$$\frac{1}{2R \log(2)} \left(\frac{1}{1/\text{snr} + E} - \frac{1/\text{snr} + 1}{(1/\text{snr} + E)^2} \right) = -\frac{1}{2R \log(2)} \frac{1}{(1/\text{snr} + E)^2} \quad (172)$$

which happens when $E = 0$. Hence, there is another minimum with zero error. Let us determine which of these two is dominant. We have:

$$\phi(0) = -\frac{1}{2R \log(2)} (\log(1/\text{snr}) + \text{snr}) + \frac{\text{snr}}{2R \log(2)} = \frac{\log_2(\text{snr})}{2R} \quad (173)$$

$$\phi(1) = -\frac{\log_2(1/\text{snr} + 1)}{2R} + 1 \quad (174)$$

so that the two are equal when:

$$\log_2(\text{snr}) = 2R - \log_2(1 + 1/\text{snr}) \quad (175)$$

or equivalently when:

$$R = \frac{1}{2} \log_2(1 + \text{snr}) = C \quad (176)$$

where we recognize the expression of the Shannon Capacity. These results are confirming that, at large value of B , the correct value of the section error rate tends to zero and to a perfect reconstruction, at least as long as the rate remains below the Shannon capacity after which, of course, this could not be true anymore. This confirms, using the replica methods, the results by [2, 3] that these codes are capacity achieving.

D. Results from the replica analysis

From this analysis, we can extract the phase diagram of the superposition codes scheme. Fig. 12 presents phase diagrams for different snr values, where the x axis is the section size B while the y axis is the distance to the capacity in dB. The blue curve is the BP threshold extracted from the potential (155) which marks the end of optimality of the AMP decoder without spatial coupling or proper power allocation, while the red curve is the optimal threshold: the best rate until decoding is theoretically possible. The black dashed curve is the asymptotic BP threshold (171).

A first observation is that the BP threshold is converging quite slowly to its asymptotic value compared to the optimal one that converges faster to the capacity. We also note that the section size where starts the transitions, and thus marks the appearance of the regime where the AMP decoder without spatial coupling is not Bayes optimal anymore, gets larger as the snr decreases. When the snr is not too large, we see that the optimal and BP thresholds almost coincide at small B values, such as for $B = 16$ at snr = 7 and $B = 4$ for snr = 15. Below this section size value, there are no more sharp phase transitions

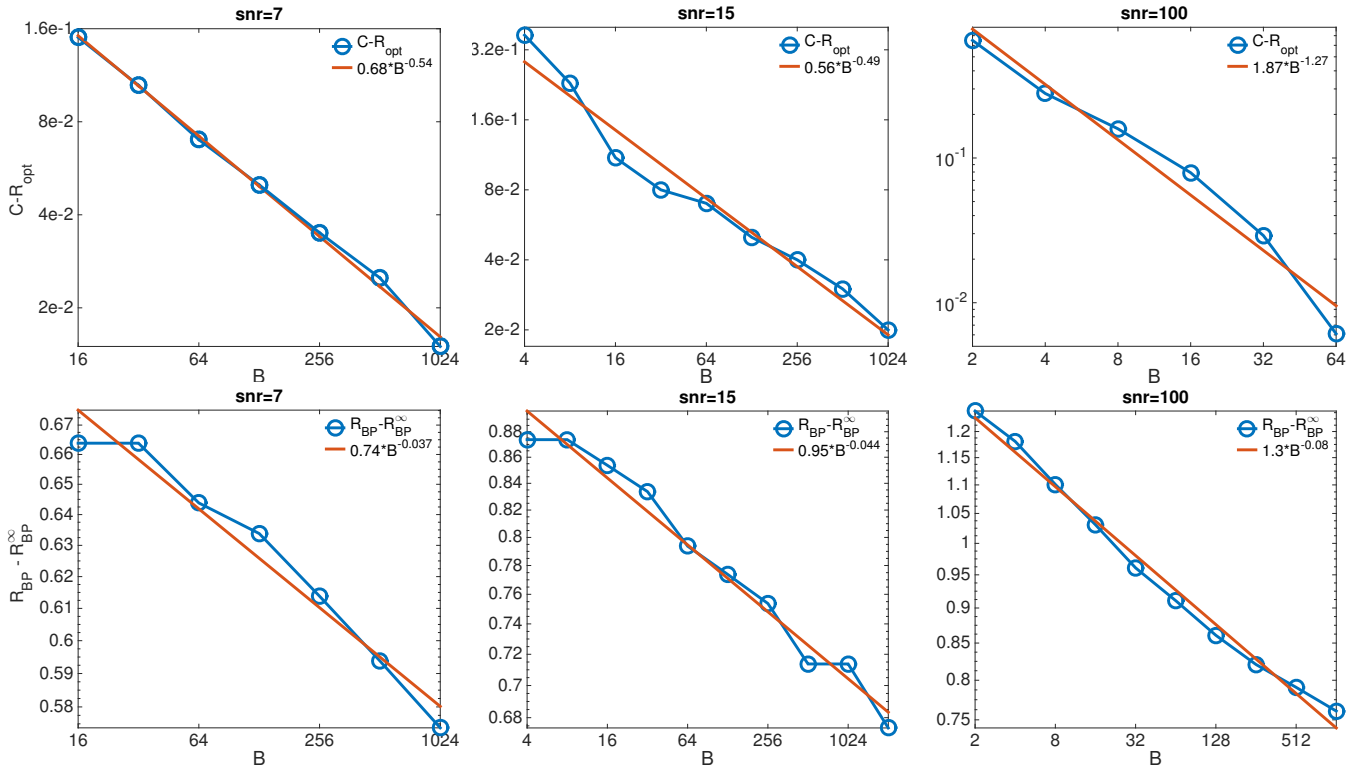


Fig. 13. In these plot we show how R_{BP} and R_{opt} change when B is increased according to the replica theory. The blue points are computed by replica method from the potential (155) where the integral is computed by monte carlo method. **Upper plots:** These pictures show how fast the optimal threshold R_{opt} is approaching the capacity as the section size B increases for different snr. We plot the difference $C - R_{opt}$ as a function of B in double logarithmic scale. The lines are guide for the eyes, and should not be taken as serious fits. They strongly suggest, however, a power law behavior. **Lower plots:** We did the same for R_{BP} . We plot the difference $R_{BP} - R_{BP}^{\infty}$ as a function of B in double logarithmic scale, where R_{BP}^{∞} is the asymptotic BP threshold computed by replica method for a given snr, see (171). In every cases, we observe a behavior quite well predicted by a power law. The lines are again guide for the eyes, and the very low values of the exponents suggest a very slow logarithmic behavior .

as only one maximum exists in the potential (155) and the decoder even without spatial coupling is optimal at any rate: The SER increases continuously with the rate. As the snr increases, the curves split sooner until they remain different $\forall B$ such as in the snr = 100 case. See Fig. 15 and Fig. 14 for more details on the achievable values of the SER.

Fig. 13 gives details on the scalings of the convergence and it seems that the rate of convergence to the asymptotic values of both thresholds can be well approximated by power laws. On Fig. 13 we present the differences between the points of Fig. 12 and their asymptotic (in B) values which are the capacity C for the optimal threshold (as shown in the previous subsection) and B_{BP}^{∞} (171) for the BP threshold. It appears that the scaling exponents increase in amplitude as the snr increases: the larger the snr, the faster the convergence to asymptotics values is.

Fig. 14 represents how the optimal SER evolves at fixed rate $R = 1.3$ and snr = 15 as a function of the section size B (left plot) and at fixed rate $R = 1.3$ and $B = 2$ as a function of the section size snr (right plot). In both cases, the curves seems to be well approximated by power laws with exponent given on the plots. The points are extracted from the replica potential (155).

Fig. 15 quantifies the optimal performance asymptotically reachable by the decoder, obtained from the state evolution analysis. We plot the base 10 logarithm of the SER corresponding to the lower SER maximum of the potential (155) as a function of the rate and the section size (again the state evolution and replica analysis are equivalent as shown in VI-B). For high noise regimes, the represented SER is always reachable by AMP without the need of spatial coupling as there is no sharp transition and it can asymptotically be reached thanks to spatial coupling. For lower noise regimes, the plotted SER matches the optimal one as long as $R < R_{opt}$ where the optimal rate corresponds to the pink line. When there is no optimal transition (before that the pink line starts), the SER is the optimal one. Fig. 14 left plot is a cut in the snr = 15 plot.

VII. OPTIMALITY OF AMP RECONSTRUCTION WITH A PROPER POWER ALLOCATION

In this section, we shall discuss a particular power allocation that allows AMP to be capacity achieving in the large size limit, without the need for spatial coupling. We shall work again in the large section size B limit.

We first divide the system into G blocks, see Fig. 10. For our analysis, each of these blocks has to be large enough and contains many sections, each of these sections being itself large so that $1 \ll B \ll L_G$, $1 \ll G$ where $L_G := L/G$ is the number of sections per group. Now, in each of these blocks, we use a different power allocation: the non zero values of the

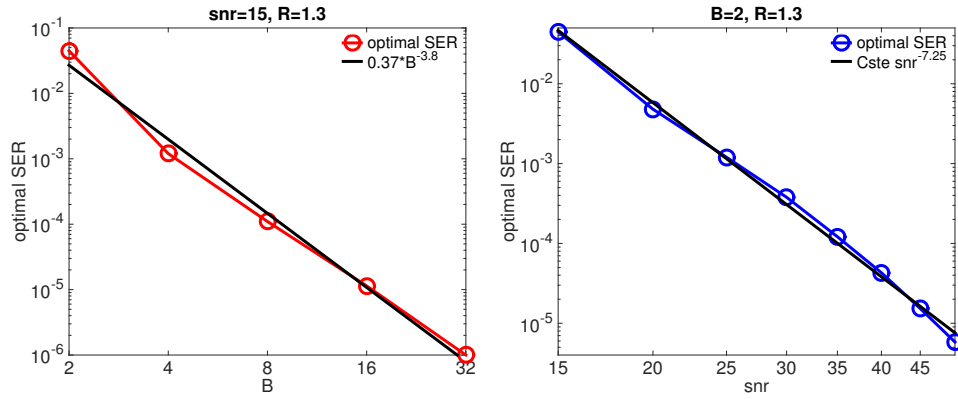


Fig. 14. In these plot we show how the optimal snr change when B is increased according to the replica theory. Both curves are plots at fixed rate $R = 1.3$ and are in double logarithmic scale. The red curve is function of B at fixed $snr = 15$, the blue one at fixed $B = 2$ as a function of the snr . The best linear fit is on the top of the curves (Cste is a constant). The points are obtained through the replica potential (155).

sections inside block g are all equal to c_g . This is precisely the case which we have studied in Sec. V-B, so we can apply the corresponding state evolution in a straightforward manner.

Our claim is that we can use the following power allocation: $c_g = \frac{2^{-Cg/G}}{Z} \forall g \in \{1, \dots, G\}$ where $C = \frac{1}{2} \log_2(1 + snr)$ is the Shannon capacity. We choose Z such that the power of the signal equals one, so that $1/G \sum_g c_g^2 = 1$. With this definition, we have:

$$Z^2 = \frac{2^{-\frac{2C}{G}} (1 - 2^{-2C})}{G(1 - 2^{-\frac{2C}{G}})} \quad (177)$$

It will be useful to know the following identity:

$$\frac{1}{G} \sum_g^{\tilde{g}} c_g^2 = \frac{1 - 2^{-\frac{2C\tilde{g}}{G}}}{1 - 2^{-2C}} \quad (178)$$

Now, we want to show that, if we have decoded all sections until the section \tilde{g} , then we will be able to decode section \tilde{g} as well. If we can show this, then starting from $\tilde{g} = 0$ we will have a succession of decoding until all is decoded, and we would have shown that this power allocation works. In this situation, using (124) and the expression of the rate R (1), we have for the section \tilde{g} :

$$(\Sigma_{\tilde{g}}^{t+1})^2 = R \log(2) \left[\frac{1/snr + \mathcal{E}_{\tilde{g}-1}}{c_{\tilde{g}}^2} \right] \quad (179)$$

with:

$$\mathcal{E}_{\tilde{g}} := 1 - \frac{1}{G} \sum_g^{\tilde{g}} c_g^2 \quad (180)$$

where we have used our assumption of having already decoded until $\tilde{g} - 1$ included: $E_g = \mathbb{I}(g \geq \tilde{g})$. (180) is the average (rescaled) biased MSE if all has been decoded until \tilde{g} , given that the initial total biased MSE is $E^0 = 1$ and that we have to remove what has been already decoded. We now ask if the block \tilde{g} can be decoded as well. The evolution of the error in this block is given by (123), and we have seen, in Sec. VI-C, that the condition for a perfect decoding in the large B limit is simply that $\Sigma^2 < 1/2$. We thus need the following to be satisfied (as long as $R < C$):

$$R \log(2) \left[\frac{1/snr + \mathcal{E}_{\tilde{g}-1}}{c_{\tilde{g}}^2} \right] < \frac{1}{2} \quad (181)$$

If this condition is satisfied, there is no BP threshold to block the AMP reconstruction in the block \tilde{g} , then the decoder will move to the next block, etc. . . . We thus needs this condition to be correct $\forall \tilde{g} \in \{1, \dots, G\}$. Let us perform the large G limit (remembering that g/G stays however finite). We have:

$$c_g^2 = \frac{G(1 - 2^{-\frac{2C}{G}})}{2^{-\frac{2C}{G}} (1 - 2^{-2C})} 2^{-\frac{2Cg}{G}} = \frac{G(1 - 2^{-\frac{2C}{G}})}{(1 - 2^{-2C})} 2^{-\frac{2C(g-1)}{G}} \quad (182)$$

$$\approx G \frac{2^{-\frac{2C(g-1)}{G}}}{(1 - 2^{-2C})} (\log(2)2C/G + O(1/G^2)) \approx \frac{2C \log(2) 2^{-\frac{2C(g-1)}{G}}}{1 - 2^{-2C}} + O(1/G) \quad (183)$$

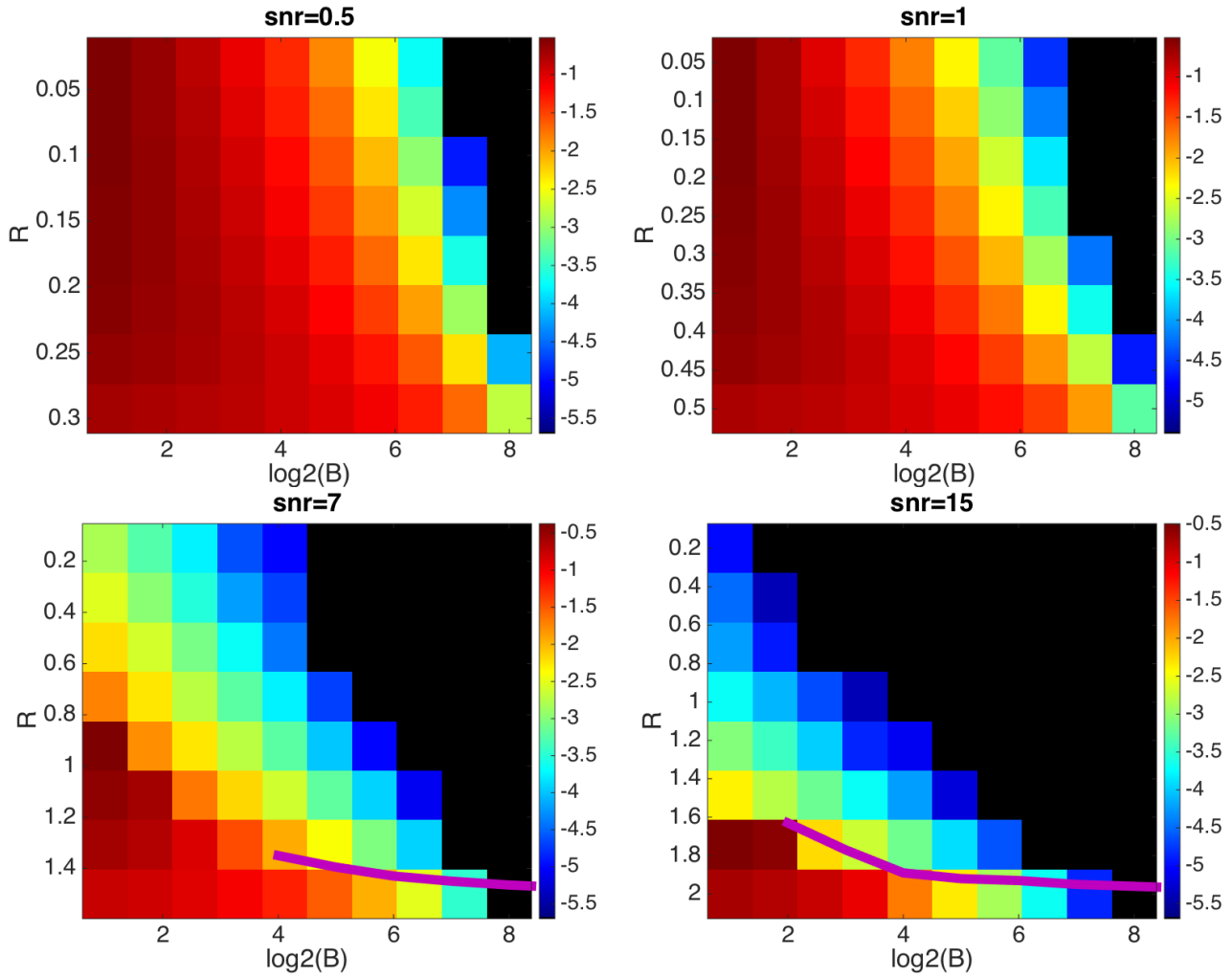


Fig. 15. On this plot, we show the logarithm in base 10 of the section error rate corresponding to the lowest SER maximum of the replica potential (155) in the (R, B) plan for different snr values. The values are obtained from the state evolution recursion (94) starting from the solution (i.e with an initial error equal to 0). The recursion (94) is computed by monte carlo method with sample size of $5B \times 10^5$. The black squares correspond to points where the computed value is SER = 0 which actually means a value that is lower to $(5 \times 10^5)^{-1}$ with high probability. The pink line in the two lower plots correspond to the optimal rate R_{opt} as in Fig. 12. In the two upper plots that correspond to high noise regimes, there is no transition at all (the AMP decoder is thus always Bayes optimal, at least for these manageable section sizes B) and the optimal SER is a smooth increasing function with the rate R at fixed B and decreasing function of B at fixed R . The SER values in the two lower plots corresponding to low noise regimes match the optimal SER as long as it is for a rate $R < R_{opt}$ lower than the optimal one. For higher rates, the maximum of the potential corresponding to the plotted SER values is not the global maximum and thus cannot be reached, even with spatial coupling that works asymptotically until the optimal rate. For B smaller than 4 (resp. 2) on the snr = 7 (resp. snr = 15) plot, there is no sharp transition and the represented SER value is the optimal one and can be reached by AMP without spatial coupling, as in the high noise regime.

Now, we note that the snr can be written as $\text{snr} = 2^{2C} - 1 = \frac{1-2^{-2C}}{2^{-2C}}$ so using (178) we have:

$$1/\text{snr} + \mathcal{E}_{\bar{g}-1} = \frac{2^{-2C}}{1-2^{-2C}} + 1 - \frac{1-2^{-\frac{2C(\bar{g}-1)}{G}}}{1-2^{-2C}} = \frac{2^{-\frac{2C(\bar{g}-1)}{G}}}{1-2^{-2C}} \quad (184)$$

Therefore to leading order, we have using (183) that:

$$\frac{1/\text{snr} + \mathcal{E}_{\bar{g}-1}}{c_{\bar{g}}^2} \approx \frac{1}{2C \log(2)} \quad (185)$$

so that the condition (181) becomes for large G :

$$\frac{R \log(2)}{2C \log(2)} = \frac{R}{2C} < \frac{1}{2} \quad (186)$$

or equivalently, $R < C$. This shows that, with proper power allocation and as long as $R < C$, there asymptotically cannot be a local minimum in the potential; or equivalently, that the AMP decoder cannot be stuck in such a spurious minimum, and it will reach the solution with perfect reconstruction SER = 0.

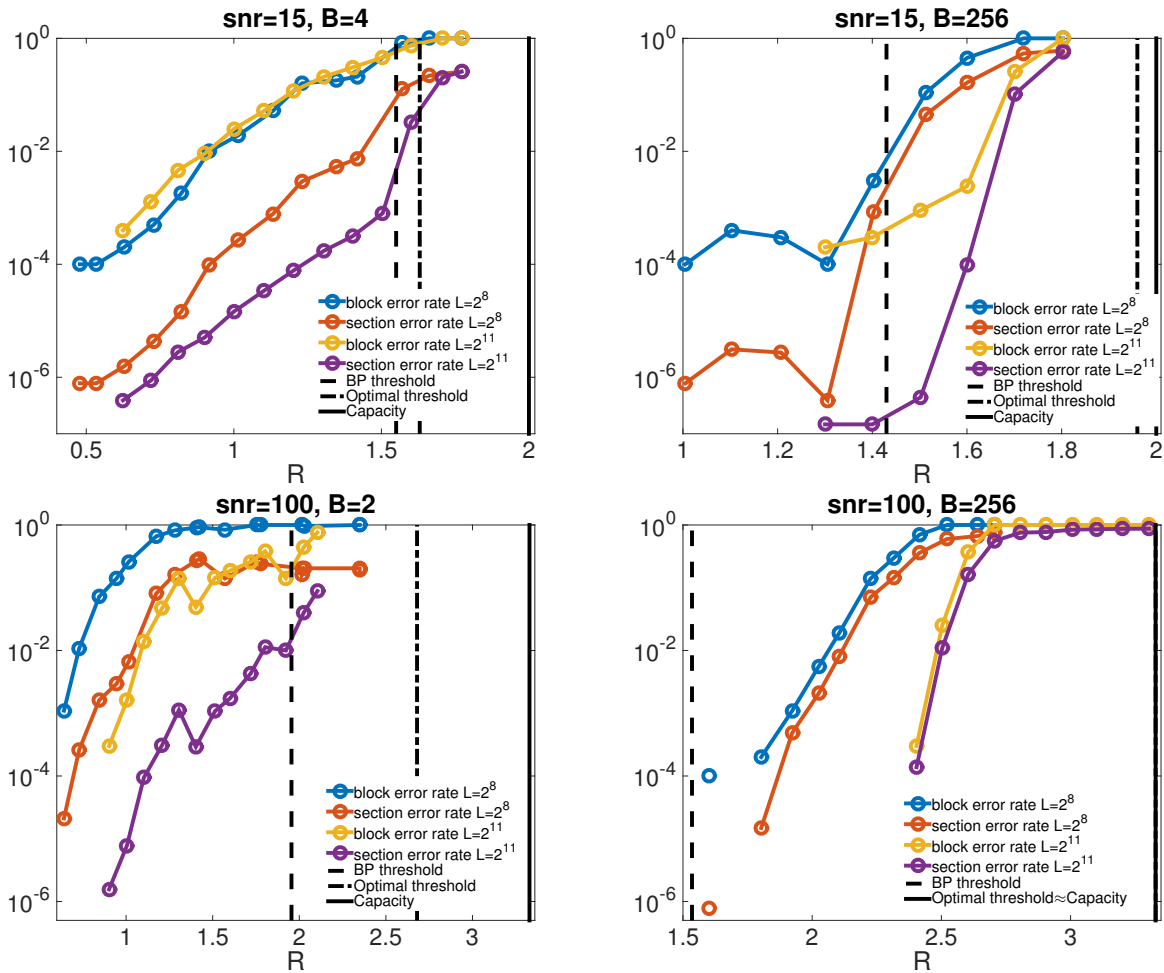


Fig. 16. On this plot, we show the block error rate and section error rate of the superposition codes using AMP combined with the spatially coupled Hadamard operator for two different snr, signal size L and section size B . The block error rate is the fraction of the 10^4 random instances we ran for each point that have not been perfectly reconstructed, i.e in these instances at least one section has not been well reconstructed ($\text{SER} > 0$). The convergence criterion is that the mean change in the variables estimates between two consecutive iterations $\delta < 10^{-8}$ and the maximum number of iterations is $t_{Max} = 3000$. The upper plots are for $\text{snr} = 100$, the lower for $\text{snr} = 15$ (notice the different x axes). The first dashed black line is the BP threshold obtained by state evolution analysis, the second one is the optimal threshold obtained by the replica method (see (155)) and the solid black line is the capacity. In the ($\text{snr} = 100, B = 256$) case, the optimal threshold is so close to the capacity that we plot a single line. For such sizes, the block error rate is 0 for rates lower than the lowest represented rate. The spatially coupled operators used for the experiment are drawn from the ensemble ($L_c = 16, L_r = 17, w = 2, \sqrt{J} = 0.4, R, \beta_{seed} = 1.8$).

VIII. NUMERICAL EXPERIMENTS FOR FINITE SIZE SIGNALS

We now present a number of numerical experiments testing the performance and behavior of the AMP decoder in different practical scenarios with finite size signals. The first experiment Fig. 16 quantifies the influence of the finite size effects over the superposition codes scheme with spatially coupled Hadamard based operators, decoded by AMP. For each plot, we fix the snr and the alphabet size B and repeat 10^4 decoding experiments with each time a different signal and operator drawn from the ensemble ($L_c = 16, L_r = 17, w = 2, \sqrt{J} = 0.4, R, \beta_{seed} = 1.8$). The curves present the block error rate (blue and yellow curves) which is the fraction of instances that have not been perfectly decoded (i.e such that the final $\text{SER} > 0$) and the SER (red and purple curves). This is done for two different sizes $L = 2^8$ and $L = 2^{11}$. When the curves stop, it means that the empirical block error rate (and thus the section error rate as well) is actually 0. In reality it should reach a noise floor $< 10^{-4}$ but does not because of the same reasons explained in Sec. IV. The dashed lines are the BP threshold R_{BP} and optimal threshold R_{opt} extracted respectively from the state evolution analysis and potential (155) and the solid black line is the capacity C . Thanks to the fact that at large enough section size B , the gap between the BP threshold and capacity is consequent, it leaves room for the spatially coupled AMP decoder to beat the transition, allowing to decode at $R > R_{BP}$ as in LDPC codes. For small section size B , the gap is too small to get real improvement over the full operators. We also note the previsible fact that as the signal size L increases, the results are improving: One can decode closer to the asymptotic transitions and reach a lower error floor. For $B = 256$, the sharp phase transition between the phases where decoding is possible/impossible by AMP with spatial coupling is clear and gets sharper as L increases.

The next experiment Fig. 17 is the phase diagram for superposition codes at fixed $\text{snr} = 15$ like on Fig. 12 but where we

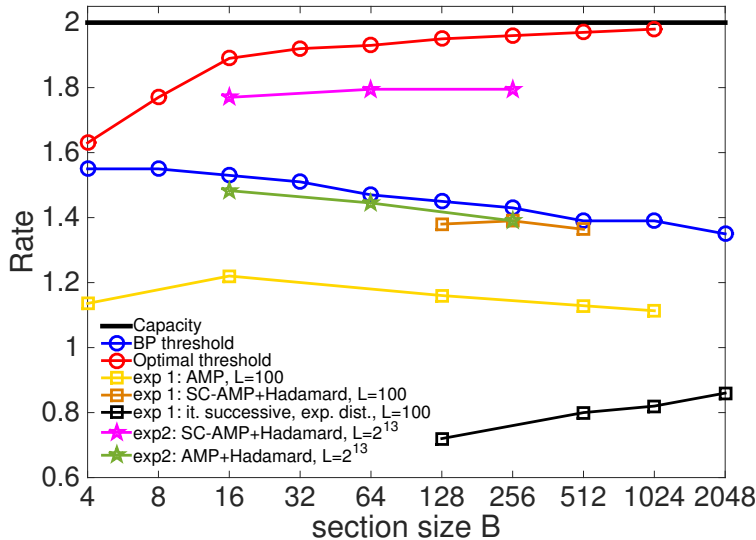


Fig. 17. Phase diagram and experimental results for superposition codes: Numerical experiment at finite size L for $\text{snr} = 15$ and asymptotic results. The solid black line is the capacity which bounds the performance of any reconstruction algorithm for this snr , the blue line is the BP threshold obtained R_{BP} by state evolution analysis and marks the limit of efficiency of AMP *without* spatial coupling for large signals and the red line is the Bayesian optimal threshold R_{opt} which is the best performance any algorithm can reach for a given section size B (obtained by the replica method, see (155)). The yellow, black and brown curves are results of the following experiment (exp 1): decode 10^4 random instances and identify the transition line between a phase where the probability p_ϵ to have a $\text{SER} > 10^{-1}$ is $p_\epsilon < 10^{-3}$ (below the line) from a phase where $p_\epsilon \geq 10^{-3}$ (more than 9 instances have failed over the 10^4 ones). The green and pink curves are the result of the second protocol (exp 2) which is a relaxed version of exp 1 with 10^2 random instances and $p_\epsilon < 10^{-1}$ below the line, $p_\epsilon \geq 10^{-1}$ above. Note that in our experiments $\text{SER} < 10^{-1}$ essentially means $\text{SER} = 0$ at these sizes. The yellow curve compares our results with the iterative successive decoder (black curve) of [2, 3] where the number of sections $L = 100$. Note that these data, taken from [2, 3], have been generated with an exponential power allocation rather than the constant one we used. Compared with the yellow curve (AMP with the same value of L) the better quality of AMP reconstruction is clear. The green and pink curves are here to show the efficiency of the Hadamard operator with AMP with (pink curve) or without (green curve) spatial coupling. For the experimental results, the maximum number of iterations of the algorithm is arbitrarily fixed to $t_{Max} = 500$. The parameters used for the spatially coupled operators are $(L_r = 16, L_c = 17, w = 2, \sqrt{J} = 0.3, R, \beta_{seed} = 1.2)$.

added on top finite size results. The asymptotic rates that can be reached are shown as a function of B (blue line for the BP threshold, red one for the optimal rate). The solid black line is the capacity. Comparing the black and yellow curves, it is clear that even without spatial coupling, AMP outperforms the iterative successive decoder of [2] for practical B values. With the Hadamard spatially coupled AMP algorithm, this is true for any B and is even more pronounced (brown curve). The green (pink) curve shows that the full (spatially coupled) Hadamard operator has very good performances for reasonably large signals, corresponding here to a blocklength $M < 64000$ (the blocklength is the size of the transmitted vector $\tilde{\mathbf{y}}$).

Finally, the last experiment is a comparison of the efficiency of the decoder combined with spatial coupling or an optimized power allocation. The optimized power allocation used here comes from [18]. We repeated their experiments and compared the results to a spatial coupling strategy. Comparing the results with Hadamard based operators, given by the red and yellow curves for power allocation and spatial coupling respectively, it is clear that spatial coupling (despite being not optimized at each rate) greatly outperforms an optimized power allocation scheme.

In addition, we see that our red curve corresponding to the optimized power allocation homogeneously outperforms the performances of [18] with exactly the same parameters, given by the blue curve. As we have numerically shown that Hadamard based operators gets same final performances as random ones as used in [18] (see [19] and Fig. 6), the difference in performances must come from the AMP implementation: In our decoder that we denote by on-line decoder, there is no need of pre-processing computations but in the decoder of [18] denoted by off-line, quantities need to be computed in advance.

The advantage of spatial coupling over power allocation is independent of the decoder and the fact that we use Hadamard operator, as it outperforms the red curve, results obtained with our on-line decoder and Hadamard operators as well. This is true at any rate except at very high values where spatial coupling does not decode at all, meanwhile the very first components of the signal are found by power allocation strategy as their power is very large. But it is not a really useful regime as only a small part of the signal is decoded anyway, even with power allocation. The green points show that a mixed strategy of spatial coupling with optimized power allocation does not perform well compared to individual strategies. This is easily understood from the Fig. 10: A power allocation modify the spatial coupling and worsen its original design. In addition we notice that at low rates, a power allocation strategy performs worst that constant power allocation.

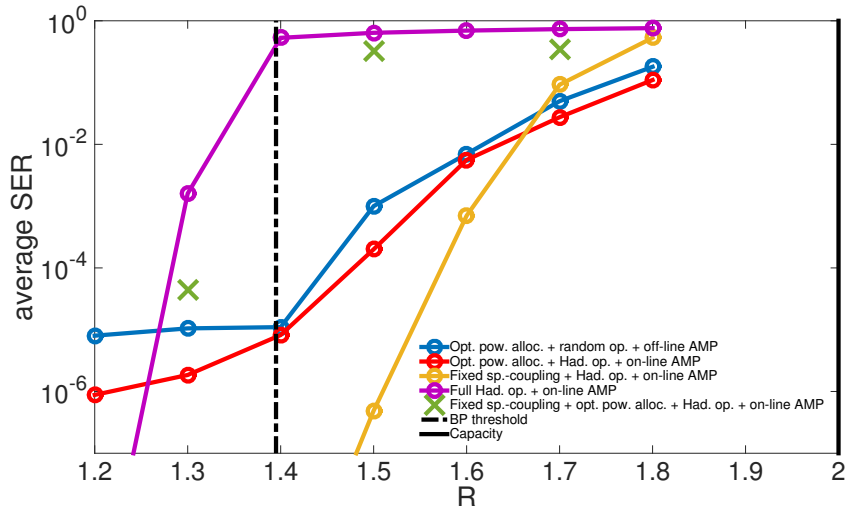


Fig. 18. The average section error rate SER in logarithmic scale as a function of the rate R for different settings, all at fixed ($\text{snr} = 15$, $B = 512$, $L = 1024$). The black dashed curve identifies the BP threshold, the best threshold until which AMP can asymptotically perform well *without* spatial coupling and constant power allocation, the black solid line is the Shannon capacity. **Blue curve:** It corresponds to the results of Fig. 3 of [18]; the points are averaged over 10^3 instances of random experiments using i.i.d Gaussian matrices and an optimized power allocation scheme where the parameters defining the power allocation are optimized for each rates. The values of the parameters and the associated power allocation scheme can be found in [18]. The denomination off-line AMP refers to the AMP decoder update rules of [18] that are different than ours and require an off-line pre-processing part as opposed to our procedure where all the quantities are computed on-line without any need of pre-processing. **Red curve:** We reproduced exactly the same experiment (with same power allocation scheme and parameters) as for the blue curve with two important differences: i) we used our on-line AMP decoder instead of their off-line implementation and ii) we used an Hadamard based full operator instead of a random i.i.d Gaussian one. In addition, we ran 10^4 instances instead of 10^3 as we had an average SER equals to 0 for the two first points. **Purple curve:** This experiment with 10^4 instances per point is with an Hadamard based full operator with on-line AMP decoding of constant power allocated signals. As it should, the decoder does not work anymore for $R > R_{BP}$. **Yellow curve:** The points of this experiment have been averaged over 10^4 points. In this setting, we used our on-line AMP decoder and generated the signals with constant power allocation. We replaced the full Hadamard operator by a spatially coupled Hadamard based operator, described in Sec. III and Fig. 5. The parameters defining the ensemble from which the operator is randomly generated are fixed once for all for the all experimental curve, as opposed to the power allocation curves where parameters have been optimized for each point. The ensemble is here given by ($L_c = 16$, $L_r = 17$, $w = 2$, $\sqrt{J} = 0.4$, R , $\beta_{\text{seed}} = 1.4$). **Green crosses:** These points have been averaged over 10^4 instances. We used the same spatially coupled Hadamard based operator ensemble as for the yellow curve for decoding power allocated signals with same power allocation scheme as the blue and red curves. When the purple and yellow curves fall, it means that the points values are 0. The codeword size for all these curves is between 5×10^3 to 9×10^3 .

IX. CONCLUSION AND FUTURE WORKS

We have fully derived and studied the approximate message passing decoder, combined with spatial coupling or power allocation, for the sparse superposition error correction scheme over the additive white Gaussian noise channel. Links have been established between the present problem and compressed sensing with structured sparsity.

On the theoretical side, we have computed the potential of the scheme under message passing decoding thanks to the heuristic replica method and have shown that the scheme is capacity achieving in a proper limit. The analysis shows that there exists a sharp phase transition blocking the decoding by message passing before the capacity but that the optimal Bayesian decoder obtained by combining message passing to spatial coupling or power allocation can reach the capacity as the section size of the signal increases. We have also derived the state evolution recursions associated to the message passing decoder, with or without spatial coupling and power allocation. The replica and state evolution analysis have been shown to be perfectly equivalent for predicting the various phase transitions as the state evolution recursions can be derived as fixed point equations of the replica potential. The optimal performances have been studied and it appeared that the error decrease and the rates of convergence of the various transitions to their asymptotic values follow power laws.

On the more practical and experimental side, we have presented an efficient and capacity achieving solver based on spatially coupled fast Hadamard operators. It allows to deal with very large instances and performs as well as random coding operators. Intensive numerical experiments show that a well designed spatial coupling performs way better than an optimized power allocation of the signal, both in terms of reconstruction error and robustness to noise. Finite size performances of the decoder under spatial coupling have been studied and it appeared that even for small signals, spatial coupling allows to obtain very good performances. In addition, we have shown that the message passing decoder without spatial coupling beats the iterative successive decoder of Barron and Joseph for any manageable size and that its performances with spatial coupling are way better for any section size.

The scheme should be now compared in a more systematic way to other state-of-the-art error correction schemes over the additive white Gaussian noise channel. On the application side, from the structure of the reconstructed signal itself in superposition codes, we can also interpret the problem as a structured group testing problem where one is looking for the only individual that has some property (for example infected) in each group. We plan to look at these questions in future works.

ACKNOWLEDGMENTS

The research leading to these results has received funding from the European Research Council under the European Union's 7th Framework Programme (FP/2007-2013/ERC Grant Agreement 307087-SPARCS and from the French Ministry of defense/DGA. We want to thank Rüdiger Urbanke for useful discussions.

REFERENCES

- [1] J. Barbier and F. Krzakala, "Replica analysis and approximate message passing decoder for superposition codes," *arXiv preprint arXiv:1403.8024*, 2014.
- [2] A. R. Barron and A. Joseph, "Sparse superposition codes: Fast and reliable at rates approaching capacity with gaussian noise," *Manuscript. Available at "http://www.stat.yale.edu/arb4"*, 2010.
- [3] —, "Analysis of fast sparse superposition codes," in *Information Theory Proceedings (ISIT), 2011 IEEE International Symposium on*. IEEE, 2011, pp. 1772–1776.
- [4] A. Joseph and A. R. Barron, "Least squares superposition codes of moderate dictionary size are reliable at rates up to capacity," *Information Theory, IEEE Transactions on*, vol. 58, no. 5, pp. 2541–2557, 2012.
- [5] A. R. Barron and S. Cho, "High-rate sparse superposition codes with iteratively optimal estimates," in *Information Theory Proceedings (ISIT), 2012 IEEE International Symposium on*. IEEE, 2012, pp. 120–124.
- [6] S. Cho and A. Barron, "Approximate iterative bayes optimal estimates for high-rate sparse superposition codes."
- [7] T. Richardson and R. Urbanke, *Modern Coding Theory*. Cambridge University Press, 2008.
- [8] S. Kudekar, T. Richardson, and R. Urbanke, "Spatially coupled ensembles universally achieve capacity under belief propagation," 2012, arXiv:1201.2999v1 [cs.IT].
- [9] S. Kudekar, T. J. Richardson, and R. L. Urbanke, "Threshold saturation via spatial coupling: Why convolutional ldpc ensembles perform so well over the bec," *Information Theory, IEEE Transactions on*, vol. 57, no. 2, pp. 803–834, 2011.
- [10] S. Kudekar and H. Pfister, "The effect of spatial coupling on compressive sensing," in *Communication, Control, and Computing (Allerton)*, 2010, pp. 347–353.
- [11] F. Krzakala, M. Mézard, F. Sausset, Y. Sun, and L. Zdeborová, "Statistical physics-based reconstruction in compressed sensing," *Phys. Rev. X*, vol. 2, p. 021005, 2012.
- [12] F. Krzakala, M. Mézard, F. Sausset, Y. Sun, and L. Zdeborová, "Probabilistic reconstruction in compressed sensing: Algorithms, phase diagrams, and threshold achieving matrices," *J. Stat. Mech.*, 2012.
- [13] D. L. Donoho, A. Javanmard, and A. Montanari, "Information-theoretically optimal compressed sensing via spatial coupling and approximate message passing," in *Proc. of the IEEE Int. Symposium on Information Theory (ISIT)*, 2012.
- [14] D. Donoho, A. Maleki, and A. Montanari, "Message passing algorithms for compressed sensing: I. motivation and construction," in *IEEE Information Theory Workshop (ITW)*, 2010, pp. 1–5.
- [15] A. Montanari, "Graphical models concepts in compressed sensing," *Compressed Sensing: Theory and Applications*, pp. 394–438, 2012.
- [16] M. Bayati and A. Montanari, "The dynamics of message passing on dense graphs, with applications to compressed sensing," *IEEE Transactions on Information Theory*, vol. 57, no. 2, pp. 764–785, 2011.
- [17] R. G. Baraniuk, V. Cevher, M. F. Duarte, and C. Hegde, "Model-based compressive sensing," *CoRR*, vol. abs/0808.3572, 2008. [Online]. Available: <http://arxiv.org/abs/0808.3572>
- [18] C. Rush, A. Greig, and R. Venkataramanan, "Capacity-achieving sparse superposition codes via approximate message passing decoding," *arXiv preprint arXiv:1501.05892*, 2015.
- [19] J. Barbier, F. Krzakala, and C. Schülke, "Approximate message-passing with spatially coupled structured operators, with applications to compressed sensing and sparse superposition codes," *arXiv preprint arXiv:1312.1740*, 2013.
- [20] A. Javanmard and A. Montanari, "State evolution for general approximate message passing algorithms, with applications to spatial coupling," *Information and Inference*, p. iat004, 2013.
- [21] M. Mézard, G. Parisi, and M. A. Virasoro, *Spin-Glass Theory and Beyond*. Singapore: World Scientific, 1987, vol. 9.
- [22] M. Mézard and A. Montanari, *Information, Physics, and Computation*. Oxford: Oxford Press, 2009.
- [23] C. Shannon, "A mathematical theory of communication," *Bell System Technical Journal*, vol. 27, pp. 379–423, 623–656, 1948.
- [24] D. L. Donoho, "Compressed sensing," *IEEE Trans. Inform. Theory*, vol. 52, p. 1289, 2006.
- [25] S. Rangan, "Generalized approximate message passing for estimation with random linear mixing," in *IEEE International Symposium on Information Theory Proceedings (ISIT)*, 2011, pp. 2168–2172.
- [26] J. Barbier, F. Krzakala, M. Mézard, and L. Zdeborová, "Compressed sensing of approximately-sparse signals: Phase transitions and optimal reconstruction," in *50th Annual Allerton Conference on Communication, Control, and Computing*, 2012.
- [27] J. Barbier, F. Krzakala, L. Zdeborová, and P. Zhang, "Robust error correction for real-valued signals via message-passing decoding and spatial coupling," *CoRR*, vol. abs/1304.6599, 2013. [Online]. Available: <http://arxiv.org/abs/1304.6599>
- [28] S. Rangan, "Generalized approximate message passing for estimation with random linear mixing," in *Information Theory Proceedings (ISIT), 2011 IEEE International Symposium on*. IEEE, 2011, pp. 2168–2172.
- [29] E. B. Sudderth, A. T. Ihler, M. Isard, W. T. Freeman, and A. S. Willsky, "Nonparametric belief propagation," *Communications of the ACM*, vol. 53, no. 10, pp. 95–103, 2010.
- [30] H. Nishimori, *Statistical Physics of Spin Glasses and Information Processing*. Oxford: Oxford University Press, 2001.
- [31] P. Schniter and S. Rangan, "Compressive phase retrieval via generalized approximate message passing," in *Communication, Control, and Computing (Allerton), 2012 50th Annual Allerton Conference on*. IEEE, 2012, pp. 815–822.
- [32] C. Wen and K. Wong, "Analysis of compressed sensing with spatially-coupled orthogonal matrices," *CoRR*, vol. abs/1402.3215, 2014. [Online]. Available: <http://arxiv.org/abs/1402.3215>
- [33] A. Javanmard and A. Montanari, "Subsampling at information theoretically optimal rates," 2012, arXiv:1202.2525v1 [cs.IT].
- [34] T. T. Do, T. D. Tran, and L. Gan, "Fast compressive sampling with structurally random matrices," in *Acoustics, Speech and Signal Processing, 2008. ICASSP 2008. IEEE International Conference on*. IEEE, 2008, pp. 3369–3372.
- [35] T. Tanaka, "A statistical-mechanics approach to large-system analysis of cdma multiuser detectors," *Information Theory, IEEE Transactions on*, vol. 48, no. 11, pp. 2888–2910, 2002.
- [36] H. Nishimori, *Statistical physics of spin glasses and information processing*. Oxford University Press Oxford, 2001, vol. 187.
- [37] B. Derrida, "Random-energy model: Limit of a family of disordered models," *Physical Review Letters*, vol. 45, no. 2, pp. 79–82, 1980.
- [38] G. B. Arous, L. V. Bogachev, and S. A. Molchanov, "Limit theorems for sums of random exponentials," *Probability theory and related fields*, vol. 132, no. 4, pp. 579–612, 2005.